# A Google Earth Engine Tool for Mapping Key Metrics of Glacier Health from Space

| | |
|---|---|
| Journal: | *Journal of Glaciology* |
| Manuscript ID | JOG-2026-0051 |
| Manuscript Type: | Article |
| Date Submitted by the Author: | 14-Apr-2026 |
| Complete List of Authors: | Lamantia, Kara; University of Bristol, School of Geographical Sciences<br>Larocca, Laura; Arizona State University, School of Ocean Futures<br>Aberle, Rainey; US Army Engineer Research and Development Center Cold Regions Research and Engineering Laboratory<br>Maussion, Fabien; University of Bristol, School of Geographical Sciences<br>Lea, James; University of Liverpool, Department of Geography and Planning |
| Keywords: | Glacier monitoring, Glacier mapping, Remote sensing, Mountain glaciers, Glacier mass balance |
| Abstract: | Satellite-based observations enable monitoring of glacier health metrics, essential for assessing glacier response to climate change and the environmental services they provide. Here, we present a Google Earth Engine tool for automated mapping of key climate- and mass balance-modulated parameters, including total visible ice area, snow-covered area (SCA), accumulation-area ratio, and snowline altitude (often used as a proxy for the equilibrium-line altitude). The tool uses Landsat near-infrared reflectance, commonly used spectral band ratios, and scene-specific thresholding to distinguish snow-covered from ice or firn surfaces. Validation for 60 glaciers across 13 regions shows strong agreement with manual observations of satellite imagery and weaker agreement with field-based observations from the World Glacier Monitoring Service (WGMS), likely reflecting differences in methodology and observation timing. The tool substantially improves WGMS temporal |

| | |
|---|---|
| | coverage, filling ~63% of glacier-year gaps and increasing the total number of observations (e.g., SCA by ~65%). Beyond the glaciers studied here, the tool is designed to enable efficient and accessible generation of multi-decadal glacier health time series for individual glaciers globally, with appropriate user evaluation and consideration of known limitations. Thus, the tool will hold value for a range of academic and non-academic users, particularly for education, outreach, and community stakeholders. |
| | |

# A Google Earth Engine Tool for Mapping Key Metrics of Glacier Health from Space

Kara A. Lamantia[1*], Laura J. Larocca[2*], Rainey Aberle[3], Fabien Maussion[1], James M. Lea[4]

[1]*School of Geographical Sciences, University of Bristol, Bristol, UK*
[2]*School of Ocean Futures, Arizona State University, Tempe, AZ, USA*
[3]*Cold Regions Research and Engineering Laboratory, Hanover, NH 03755, USA*
[4]*Department of Geography and Planning, University of Liverpool, Liverpool, UK*

*These authors contributed equally to this work

*Correspondence: Kara Lamantia <kara.lamantia@bristol.ac.uk>*

## Abstract

Satellite-based observations enable monitoring of glacier health metrics, essential for assessing glacier response to climate change and the environmental services they provide. Here, we present a Google Earth Engine tool for automated mapping of key climate- and mass balance- modulated parameters, including total visible ice area, snow-covered area (SCA), accumulation-area ratio, and snowline altitude (often used as a proxy for the equilibrium-line altitude). The tool uses Landsat near-infrared reflectance, commonly used spectral band ratios, and scene-specific thresholding to distinguish snow-covered from ice or firn surfaces. Validation for 60 glaciers across 13 regions shows strong agreement with manual observations of satellite imagery and weaker agreement with field-based observations from the World Glacier Monitoring Service (WGMS), likely reflecting differences in methodology and observation timing. The tool substantially improves WGMS temporal coverage, filling ~63% of glacier-year gaps and increasing the total number of observations (e.g., SCA by ~65%). Beyond the glaciers studied here, the tool is designed to enable efficient and accessible generation of multi-decadal glacier health time series for individual glaciers globally, with appropriate user evaluation and consideration of known limitations. Thus, the tool will hold value for a range of academic and non-academic users, particularly for education, outreach, and community stakeholders.



## 1. Introduction

Mountain glaciers and seasonal snowpacks act as crucial freshwater reservoirs, supplying water for irrigation, hydroelectric generation, and a wide range of ecosystem services (e.g., Immerzeel and others, 2020). In recent decades, Earth's glaciers have been losing mass at an accelerated rate, marking a retreat unprecedented in at least the last two thousand years (e.g., Hugonnet and others, 2021; Masson-Delmotte and others, 2021; Calvin and others, 2023, Larocca and others, 2023). Community estimates of global glacier mass changes since 2000 suggest that glacier mass loss is ~18% greater than that of the Greenland Ice sheet (-262 Gt $yr^{-1}$ 2002-21 versus -223 $yr^{-1}$ 2002-20, respectively) and more than twice that from the Antarctic Ice Sheet (-111 Gt $yr^{-1}$ 2002-20; Otosaka and others, 2022; The GlaMBIE Team, 2025). By 2100, global-scale projections estimate that glaciers will lose 26–41% of their mass relative to 2015, with 49–83% projected to disappear entirely (Rounce and others, 2023).

Glacier mass balance monitoring is vital for local hazard impact assessments and global climate projections (e.g., Haeberli and Whiteman, 2015; Huss and Hock, 2018; Hock and others, 2019; Hugonnet and others, 2021; Rounce and others, 2023; Ficetola and others, 2024). Notably, the major source of uncertainty in predicting near-term glacier change (i.e., to the mid twenty-first century) lies not in the emission scenario, but in the glacier models themselves (Marzeion and others, 2020; Schuster and others, 2023). These uncertainties arise in part from varying model sensitivities to air temperature and precipitation, which respectively regulate ablation and accumulation processes (Meier, 1962; Braithwaite

& Müller, 1980). As a result, improving the availability and use of observational constraints is critical for reducing uncertainty in glacier projections and their associated impacts (e.g., Wells and others, 2025).

The Randolph Glacier Inventory (RGI; RGI 7.0 Consortium, 2023) is the most widely used and globally complete glacier observational dataset, on which most global-scale projections rely to define initial condition or reference state (e.g., Huggonet and others, 2021; Rounce and others, 2023; The GlaMBIE Team, 2025). Although recently updated in 2023, the RGI represents a snapshot of the world's glaciers with a reference date of the year ~2000 (Fig. 1; Pfeffer and others, 2014; RGI Consortium, 2023). In the ~25 years since then, global temperatures have continued to rise, leading to major changes in glacier length, area, and volume worldwide (Rounce and others, 2023). As such, many glaciers have now retreated within their RGI-defined boundaries, and some have disappeared entirely (e.g., Ramírez and others, 2001; Huss at al., 2025; Van Tricht and others, 2025; Baruah and others, 2026; Serrano and others, 2026). Thus, globally consistent, time-varying glacier observations needed for glacier model calibration and evaluation are largely lacking to date.

Less than 0.2% (<500) of the world's >200,000 glaciers are monitored in situ (WGMS, 2023). Satellite-based observations offer a means to monitor key metrics of glacier health over much broader spatial scales (e.g., Rastner and others, 2019; Aberle and others, 2025). However, challenges such as cloud cover, topographic shadowing, and spectral similarities between snow, ice, and firn have complicated monitoring efforts across Earth's diverse glacierized settings (e.g., Rastner and others, 2019, Racoviteanu and others, 2019; Aberle and others, 2025). To address some of these challenges and expand accessible space-based observations of glacier state, we developed a user-friendly, open-source Google Earth Engine (GEE) tool that enables users to automatically quantify several indicators of glacier health from the year 1985 to present. Here, we use the term "glacier health" to refer to the following set of observable, satellite-derived glacier surface variables that are closely linked to climate and surface mass balance processes: the total visible ice area and snow-covered area (TA and SCA, respectively), the snowline altitude (SLA), and the accumulation-area ratio (AAR).

To validate the tool we compared our satellite-based observations (a total of 1,561 observations spanning 40 years) for a set of 60 glaciers with (1) long-term in situ field-based measurements from the World Glacier Monitoring Service (WGMS, Fig. 1), and (2) manual digitizations of end of season SCA and TA. These new data will enable direct comparisons between satellite-derived and modeled glacier-specific metrics, local climatological data, and glacier morpho-topographic variables, offering much-needed insights into glacier-climate sensitivity across diverse climate and topographic settings. The tool will also facilitate broader use of these data by non-specialist users, including educational applications.

*Figure 1 near here.*

## 2. Methods

### *2.1. Glacier health metrics*

We focus on the following four glacier health metrics which capture changes in glacier geometry and surface facies (e.g., snow-, firn- and ice-covered areas) in response to local climatic controls on accumulation and ablation (Fig. 2):

(1) snow-covered area (SCA, $km^2$), representing the zone of accumulation where mass is gained (i.e., where gain via annual snowfall exceeds melting);

(2) snowline altitude (SLA, m), defined as the lower limit of the SCA or the average elevation of the transition between snow-covered and ice- or firn-covered (ablation) surfaces (Cogley and others, 2011). When measured at the end of the balance year (and given no superimposed ice zone), the SLA may be used as a proxy for the equilibrium line altitude (ELA; e.g., Rabatel and others, 2012. 2013; Larocca and others, 2024), the elevation at which the annual net mass balance is zero (Cogley and others, 2011);

(3) total visible ice area (TA, $km^2$), representing the spatial extent of the glacier (i.e., bare ice area plus snow area, not accounting for debris covered ice); and

(4) accumulation-area ratio (AAR, unitless), defined as the ratio of the accumulation area (SCA) to the TA, for debris-free glaciers. As adjustment of glacier geometry (i.e., TA) is lagged relative to climate forcing, the AAR can indicate the extent of imbalance relative to current climatic conditions (Benn & Evans, 2010).

*Figure 2 near here.*

### *2.2. Study glaciers*

For the analyses presented here, we derived the four glacier health metrics for a set of 60 well-monitored glaciers and ice caps with long-term, field-based mass-balance observations archived by the WGMS (referred to hereafter as study glaciers; Fig. 1 and SI Table 1). This set represents a subset of the 70 glaciers reported by Ohmura and Boettcher (2022), selected based on data quality and the duration of observations (i.e., those with multi-decadal annual mass-balance records). We restrict our analysis to land-terminating (n = 45) and lake-terminating glaciers (n = 15, defined as having a lake inside or intersecting the RGI boundary), as their mass-balance and geometric changes respond more directly to atmospheric climatic forcing, in contrast to marine-terminating glaciers, where frontal ablation (e.g., calving and submarine melt) may dominate. We also note that none of the 60 study glaciers exhibit extensive debris cover.

All metrics were measured annually between 1985 and 2024 using a single satellite image per glacier and year, selected within a ±1 month window centered on the month best approximating the end of the ablation season for each location (we note that in some years, a suitable image was not available for every glacier; see Section 2.3 and SI Table 1). The target month was approximated based on region and the average survey month from which WGMS data is available. Although this sample represents only a small fraction of the world's glaciers, the selected glaciers span a wide range of geographic and climatic settings and are distributed across 13 of the 19 first-order regions defined by the RGI (Fig. 1; RGI Consortium, 2023). The subsequent validation focuses on this subset of well-observed glaciers, while the underlying methodology of the tool is designed with the broader goal of being applicable to any glacier or glacier complex within the RGI (without extensive debris cover; see Section 2.3 and 4.3).

### *2.3. Cloud-based satellite imagery analysis*

Our workflow, implemented in GEE, integrates satellite imagery across multiple sensors (Landsat 5, 7, 8, and 9) to automatically derive annual glacier-specific health metrics across a 40-year period (SI Table 2). Specifically, the algorithm integrates terrain-corrected multispectral Landsat imagery with established spectral indices, e.g., the Normalized Difference Snow Index (Dozier, 1989; Riggs and others, 1994; Hall and Riggs, 2010), band ratios, and automated thresholding techniques (Otsu segmentation; Otsu, 1979) to characterize glacier surfaces (i.e., delineate snow versus ice or firn), as described below.

To select a single image per glacier and year, we use a two-step procedure that balances image quality with seasonal representativeness. Landsat scenes are first identified within a ±1 month window centered on a target month (typically the month best representing end-of-ablation season conditions, ideally prior to accumulation season snowfall events). To prioritize the target month, the algorithm first searches within the target month only using a strict cloud-cover criterion (maximum allowable scene cloud cover minus 5 percentage points). If one or more scenes meet this criterion, the least-cloudy target-month scene is selected for that year. If no target-month scene meets the criterion, the algorithm falls back to the broader ±1 month window and selects the least-cloudy scene meeting the user-defined maximum cloud-cover threshold (Fig. 3). For example, if August is the target month and the maximum allowable cloud cover is 20%, the workflow preferentially selects August scenes with cloud cover ≤15%; if none are available for a given year, it selects the best available scene from July or September (≤20%). This approach increases the fraction of target-month acquisitions while limiting increases in average scene cloudiness. We note that Landsat 7 imagery acquired from 2003 onwards are excluded due to data gaps

associated with the Scan Line Corrector failure. Following selection of annual images, the Ekstrand correction (Ekstrand, 1996), a topographic normalization technique, is applied to account for illumination differences arising from sun elevation, incidence angle, and terrain shadowing, typical of mountainous glacierized environments (SI Fig. 1). Maximum cloud cover and minimum sun angle were set to 20% and 20°, respectively, for the 60 glaciers studied.

Following terrain correction, a masking procedure adapted from Moussavi and others (2020) is applied to reduce misclassification from surrounding rock and water surfaces. The masking is based on a thermal infrared–to–blue band reflectance ratio combined with a blue reflectance threshold. Because the original masking approach was optimized for seawater, and glacial lakes are often brighter due to suspended rock flour, multiple threshold combinations were evaluated to balance removal of surrounding rock and glacial lakes while minimizing over-masking of true snow and ice glacier surfaces. Based on this evaluation, a thermal/blue ratio >0.9 and blue <0.2 threshold was found to be most effective and is hereafter referred to as the *moderate* masking option (see Section 2.4; SI Fig. 2). In most cases masking was set to *Off* or the *moderate* option (the latter for study glaciers that terminate in or near a lake; see SI Table 1).

*Figure 3 near here.*

Following masking, each terrain-corrected image is used to derive the four primary metrics of glacier health: SCA, SLA, TA, and AAR. TA is calculated using a dual-threshold approach combining the NDSI >0.4 and a near-infrared (NIR)–to–shortwave infrared (SWIR) reflectance ratio (NIR/SWIR1 >1.4) to distinguish snow- and visible ice-covered glacier area from water, rock, and bare earth surfaces.

Next, the SCA is derived using Otsu's thresholding method applied to terrain-corrected NIR reflectance (Fig. 4a). This approach identifies an image-specific reflectance threshold from each NIR histogram and is used to distinguish snow-covered from bare ice pixels within the previously defined total glacier area (Fig. 4b; Otsu, 1979; Rastner and others, 2019). Importantly, this approach extends beyond the limitations of visible light by exploiting contrasts in NIR reflectance where snow reflects strongly and bare ice is more absorptive (Warren, 2019). This allows snow-covered and bare ice boundaries to be identified even when they are not visibly discernible. Moreover, the Otsu-derived threshold is image-specific, avoiding reliance on a fixed reflectance threshold that may not perform consistently across different images and glacier settings.

Glacier areas (TA and SCA) are calculated by summing classified pixels multiplied by pixel area (30 m resolution) and are reported in square kilometers. Next, the AAR is calculated as the ratio of the SCA to the TA. Cases in which the derived SCA exceeds the TA (i.e., AAR > 1) are identified as physically invalid and excluded from all exported outputs and subsequent analyses. Finally, the SLA is determined by identifying the glacier elevation that corresponds to the fraction of glacier area lying below the snowline (i.e., 1 − AAR). For example, for a glacier with an AAR of 0.6, the SLA corresponds to the elevation at which 40% of the total glacier area lies below, equivalent to the 40th percentile of the glacier's area–elevation distribution. We note that in the case where the entire glacier surface is ice-covered (i.e., AAR = 0), the SLA will correspond to the 100th percentile of the glacier's area-elevation distribution. Glacier elevations used in the SLA calculation were obtained from either the ArcticDEM (2 m mosaic; Porter and others, 2023) or the Copernicus GLO-30 DEM (COPDEM; European Space Agency, 2024), depending on data availability for each glacier location (SI Table 1). Both products are multi-temporal composites with acquisition periods spanning ~2007-2024 and ~2010-2015, respectively.

For each glacier and year analyzed, the tool generates a suite of geospatial and tabular outputs. Specifically, the algorithm outputs include (1) a CSV file containing annual glacier metrics (TA, SCA, AAR, and SLA) with associated uncertainties (see Sections 2.5 and 3.1) and satellite imagery metadata, (2) annual TA and SCA polygon shapefiles (Fig. 4b), and (3) CSV files reporting annual TA and SCA area-elevation distribution that may be used for hypsometric curves (i.e., pixel counts aggregated into 50 m elevation bins).

*Figure 4 near here.*

### *2.4. The Graphical User Interface*

The graphical user interface (GUI) allows users to specify key processing parameters, enabling customization of the workflow for individual glaciers with step-by-step instructions available via a GitHub repository (see Data Availability Statement). Upon loading, the GUI prompts the user to select either the RGI glacier product or the RGI glacier complex product. The latter product is new to RGI v7.0 and merges connected glaciers into one entity, while in the former, individual glaciers are represented separately (RGI Consortium, 2023). Once the selected dataset is loaded, the GUI enables the user to select the glacier of interest by clicking within its boundary. Clicks outside a glacier outline trigger an error notification indicating that no glacier has been selected, prompting the user to repeat the selection. Once selected, the algorithm highlights the glacier of interest, and a default 50 m buffer is applied to the glacier outline. This buffer can be adjusted by the user from 0 to 200 m in 50 m increments. To prevent inclusion of areas belonging to neighboring glaciers, outlines are clipped along shared boundaries, such that buffering is applied only to boundaries unique to the glacier of interest. Since the RGI represents a temporal snapshot of global glacier extent centered roughly around the year 2000 and our workflow derives glacier health metrics beginning in 1985, the buffer ensures the inclusion of ice outside the RGI margins during years prior to the outline source date.

In the GUI (SI Fig. 3), the left panel provides user controls for specifying imagery acquisition parameters (*Collect Imagery*) and processing options (*Processing Options*; Table 1). Required inputs for imagery collection include a glacier name or ID (used for export file naming), the start and end years of interest, a target month (1–12; typically corresponding to the month best representing the end of the melt season), the maximum allowable cloud cover (0–100%), and the minimum sun angle (0–90°). By default, the maximum end year corresponds to the most recent year of available imagery (e.g., 2026, at present). Once imagery is collected, the console (right panel) reports the total number of candidate images (i.e., images that meet the user-defined criteria), as well as metadata (cloud-cover percentage) for the annually selected images, chosen as the least-cloudy scene. The map view displays the glacier outline as the region of interest (ROI) and the earliest annually selected image rendered in true-color (RGB). We note that imagery acquisition parameters can be modified, and the procedure repeated, to evaluate alternative image selections under different criteria.

Following imagery selection, users specify the digital elevation model (DEM; either the COPDEM or ArcticDEM) and the rock/water masking strength under *Processing Options*. A validation check confirms that the selected DEM covers the ROI. The rock/water masking may be applied using one of three predefined levels: *light*, *moderate*, and *high*, corresponding to progressively stricter masking. The *light* level applies a thermal-to-blue reflectance ratio threshold of >0.9 and a reflectance threshold of <0.1; the *moderate* level applies a thermal-to-blue ratio of >0.9 and a blue threshold of <0.2; and the *high* level applies a thermal-to-blue ratio of >0.85 and blue threshold of <0.2. Rock/water masking can also be disabled if not required using the *Off* option (SI Fig. 2). Once *Run Analysis* is initiated, the algorithm is executed using the specified parameters. Derived glacier health metrics for the first annually selected image are reported within a feature collection in the console, and the corresponding SCA and TA masks are displayed in the map view. The analysis can be re-run after modifying the selected parameters. Each new execution refreshes the map layer and new results are reported in the console. All outputs generated by the analysis are listed in the Tasks tab and can be run individually to export results to Google Drive.

*Table 1 near here.*

### *2.5. Tool validation and uncertainty*

To evaluate the performance of the GEE-based tool (hereafter we use *GEE* and *tool* interchangeably) and estimate uncertainty, we compare annual glacier health metrics derived from the tool with observations from the WGMS and with manually digitized data for the 60 study glaciers. Specifically, tool-derived metrics are compared with the following annual WGMS field-measured observations when available (from the 2024 Fluctuations of Glaciers Database *mass_balance_overview.csv* and *mass_balance.csv* files; WGMS, 2024*)*: ELA (mean elevation averaged over the glacier, of the end-of-mass-balance-year equilibrium line, m), accumulation area ($km^2$), ablation area ($km^2$), and annual balance (mass balance over the hydrological year; mm w.e. ~ kg $m^{-2}$). We also compute WGMS TA ($km^2$) as the sum of the accumulation and ablation areas and WGMS AAR (unitless) as the accumulation area divided by the TA. We assume annual WGMS observation dates from the survey date (YYYYMMDD) in the *state.csv* file when available. In addition, we compare our tool-derived SLA estimates with ELAs reported by Ohmura and Boettcher (2022), which have been quality-checked and, where possible, infilled using the relationship between ELA and annual net mass balance.

To provide an independent benchmark for evaluating tool performance, manual digitizations were conducted for a subset of glacier–year combinations. For each of the 60 study glaciers, four Landsat scenes were randomly selected from the set of images analyzed by the tool. Using these images (n = 240) and their corresponding RGI outlines, SCA and TA were manually delineated as polygons using false-color Landsat imagery (NIR–red–green composites; SI Fig. 4). SLA was subsequently calculated from the manually digitized polygons using the same DEM-based percentile method applied in the tool workflow, and AAR was calculated as the ratio of manually derived SCA to TA.

Tool performance was quantified using the mean bias, root-mean-square error (RMSE), mean absolute error (MAE), and Pearson correlation coefficient ($r$) between tool-derived and reference values (WGMS and manual). Uncertainty in tool-derived glacier health metrics was defined from comparisons with manual digitizations only (see Section 4.1). Specifically, for each metric, uncertainty was quantified as the median absolute percent difference between tool-derived and manually digitized values across all glacier–year pairs. The resulting values are applied as fixed percentage uncertainties for all tool-exported values. For example, a tool-derived TA (±3%) of 50 $km^2$ is reported with an uncertainty of ±1.5 $km^2$, while a TA of 10 $km^2$ is reported with an uncertainty of ±0.3 $km^2$ (see Results 3.1).

In addition, we assess and compare tool- and WGMS-derived changes in glacier area over the 40-year period across the 60 study glaciers and compare tool-derived metrics with annual mass balance from the WGMS. Because the study glaciers differ in size, geometry, and climatic setting, TA and SCA values are normalized within each glacier relative to the median of all available observations within the 1985–2024 period. Values are expressed as percent change relative to this baseline and summarized across glaciers for each year using the median and interquartile range (IQR). SLA/ELA data are analyzed as anomalies relative to the same baseline period. Lastly, to quantify how well our tool-based observations complement WGMS field-based monitoring, we assess the extent to which tool-derived metrics fill temporal gaps in WGMS records for the same glaciers.

## 3. Results

### *3.1. Tool validation and uncertainty*

SLA/ELA shows the strongest agreement among the four metrics for the tool-derived–WGMS comparisons ($r$ = 0.99; Table 2 and SI Fig. 5). However, the relationship is weaker when SLA/ELA values are expressed as an anomaly relative to each glacier's median tool-derived SLA ($r$ = 0.18; Fig. 5). A modest negative bias (−146 m) suggests that tool-derived SLAs are, on average, lower than WGMS ELAs. Tool-derived estimates of SCA and TA also agree well with WGMS observations of accumulation area ($r$ = 0.89) and total area (computed as the sum of the reported accumulation and ablation areas; $r$ = 0.97), in absolute terms, but correlations are much weaker when values are normalized to account for

between-glacier differences in size ($r$ = 0.07 and $r$ = 0.05, respectively). Mean biases suggest GEE generally overestimates SCA and TA relative to WGMS (+ 2.3 km$^2$ and + 0.1 km$^2$, respectively). Because glacier size varies across the study sample, we also report median absolute percent differences of 53% for SCA and 13% for TA.

Comparison with manually digitized data demonstrates strong agreement across all glacier health indicators. Tool-derived SLA shows a strong correlation with manual SLA estimates in absolute terms ($r$ = 0.99) and when values are expressed as anomalies ($r$ = 0.77), with a small bias of −0.8 m and an RMSE of 88.2 m. SCA and TA also show excellent agreement with manual observations in absolute terms ($r$ = 0.99 and $r$ = 0.99, respectively) and when values are normalized to account for between-glacier differences in size ($r$ = 0.85 and $r$ = 0.64, respectively). Biases of + 0.2 km$^2$ and −0.3 km$^2$ indicate an overestimation of SCA and underestimation of TA relative to manual digitizations. Based on comparisons with manual digitizations, typical relative uncertainties (derived from median absolute percent differences) in the tool-derived metrics are estimated to be ±1% for SLA, ±7% for SCA, and ±3% for TA.

We also compare per-glacier WGMS- and GEE-derived glacier health metrics (TA and SCA, percent change to baseline; SLA/ELA, anomaly in m) with WGMS records of annual mass balance (Fig. 6 and SI Fig. 6). Median per-glacier Pearson correlation coefficients (r) are: TA ($r$ = 0.33, 0.28), SCA ($r$ = 0.30, 0.90), and SLA/ELA ($r$ = −0.23, −0.89), for GEE and WGMS, respectively. Overall, the GEE tool performs well, even after accounting for between-glacier differences in size and elevation, with strongest overall agreement with manual digitizations. We note that agreement is overall weaker for GEE tool–WGMS comparisons, however this could be due to a variety of reasons including methodological differences between the two datasets (see Discussion 4.1.).

*Table 2 near here.*

*Figure 5 near here.*

### *3.2. Change in glacier area over time*

Across the 60 study glaciers, both the GEE tool-derived and WGMS observations indicate substantial long-term changes in glacier area (Fig. 6a). Linear regression of annual median values (summarized across glaciers) indicates a tool-derived decline in SCA of 4.6% per decade ($p$ < 0.001), corresponding to a total decrease of ~18% over the four-decade study period. In contrast, WGMS observations indicate a much stronger decline of 17% per decade ($p$ < 0.001), equivalent to an ~66% reduction. TA shows a more gradual decline and better agreement between datasets, with trends of −3.7% per decade ($p$ < 0.001; total −14.5%) and −5.0% per decade ($p$ < 0.001; total −19.4%) for GEE and WGMS, respectively.

In general, temporal trends in glacier area metrics derived from WGMS observations are steeper than those derived from the GEE tool, particularly for SCA, likely reflecting differences in observation timing within the ablation season between the two datasets (see Discussion section 4.1.). Despite these differences, both datasets indicate declining glacier area (with TA lagged relative to SCA) between 1985 and 2024.

*Figure 6 near here.*

WGMS is an invaluable resource for glacier monitoring, however, even for well-studied glaciers, temporal gaps exist. Considering all glacier–year combinations across the 60 study glaciers and 40-year period (2400 potential observations), the GEE tool returns results for ~65% of cases (1561 observations). Across the glaciers analyzed here, the tool provides an observation for ~63% of glacier–year combinations in which the corresponding WGMS record is missing. In total, the tool yields 916 and 238 additional observations of SCA and ELA, respectively, substantially increasing the total number of

available observations. For example, over the past four decades, the tool increases the number of available SCA observations by ~65% (Fig. 7), demonstrating the potential for satellite-derived observations to augment WGMS records (although it is important to note that these data are not strictly equivalent).

*Figure 7 near here.*

## 4. Discussion

### *4.1. Interpreting differences between satellite-derived and field observations*

Overall, the tool reliably captures glacier surface conditions from optical satellite imagery and agrees well with manually derived metrics (see Section 3.1.), supporting the underlying methodology and the use of the tool for generating observational data for unmonitored glaciers. However, we observe a weaker overall agreement between the GEE tool-derived glacier health metrics and WGMS records than with our manual digitizations. We suggest that this is likely reflective of methodological differences and temporal mismatches between the satellite-derived and field-based observations.

WGMS observations are compiled from a global network of investigators and are primarily obtained using distributed ablation stakes and snow pits taken as point measurements and inter-/extrapolated across the glacier surface, from which quantities such as ELA and AAR are derived (Zemp and others, 2009). Survey platform methods for WGMS measurements of glacier length, area, and elevation range also vary between investigators and glaciers (e.g., terrestrial, airborne, spaceborne). In contrast, the tool derives annual space-based glacier health metrics from spatially continuous classifications of glacier surface conditions. Additionally, we use the RGI v7.0 outlines with a 50 m buffer applied. Although this likely captures past (pre-2000) glacier extents, the resulting maximum boundary is fixed in time and does not account for any extents beyond this boundary.

Field-based surveys are typically conducted near the end of the mass-balance year, usually at the end of the ablation season when the mass of the glacier is at the annual minimum (Cogley and others, 2011). In comparison, the tool relies on a single annual satellite image selected to best approximate end-of-ablation season conditions. However, accurately capturing end of the ablation season conditions is limited by Landsat's revisit interval (i.e., temporal resolution of ~16 days), frequent cloud cover, and GEE memory limitations, which together restrict the ability to analyze multiple images per year. As a result, WGMS accumulation and ablation area observations may not be directly comparable with single-date satellite observations (mean temporal offset, GEE − WGMS, is ~21 days; SI Fig. 7). Thus, our comparisons may involve non-coincident observations (e.g. a late-August satellite image compared with a mid-September field survey). Further, in years with late-summer or early-fall snowfall events, satellite scenes may depict snow-covered glacier surfaces that do not represent true end-of-balance-year conditions.

These temporal mismatches are most problematic for variables that rely on the position of the snowline (ELA/SLA, SCA, and AAR) as it migrates upward through the melt season (e.g., Mernild and others, 2013). This limitation has been noted in other studies that have mapped snow extent on glaciers using multi-temporal Landsat satellite imagery (e.g., Rastner and others, 2019; Larocca and others, 2024). In addition to these temporal limitations, we note that the SLA is not always strictly equivalent to the ELA (i.e., in cases where there is a superimposed ice zone; Cogley and others, 2011). We also note that for comparisons to the mass balance data, it is natural the WGMS dataset has a much higher agreement as the mass balance dataset is supplied through the WGMS database, reflecting internal consistency and not necessarily independent validation.

The data provided by the WGMS are geographically biased to the Northern Hemisphere and are subject to occasional errors, inaccuracies, and missing metadata (e.g., Zemp and others, 2009; Ohmura and Boettcher, 2022). The set of glaciers used to evaluate the performance of the GEE tool reflect this same uneven global distribution, as they were selected from the small subset of glaciers worldwide that possess long-term field-based records. In a review of the worldwide monitoring network, Zemp and

others (2009) suggest that WGMS data may contain difficult-to-quantify systematic and random errors and that these data should therefore be quality-checked against related literature prior to use. In our analysis, obvious errors (e.g. misplaced or missing decimal points, and all reported zeros in accumulation area) were corrected or excluded where possible before comparison with the satellite-derived data. Zemp and others (2009) also suggest that the accuracy of the summer balance and ablation-area observations generally exceeds that of the winter balance and the accumulation-zone observations. This could partially explain the weaker agreement between WGMS accumulation-area observations and tool-derived estimates of SCA.

### *4.2. Tool limitations*

The spectral characteristics of seasonal snow, glacier ice, and firn are similar in optical satellite imagery, with the reflectance signatures of snow and firn exhibiting the greatest overlap (e.g., Fig. 1 in Aberle and others, 2025). This similarity can complicate glacier snow cover mapping because misclassification of firn as snow can lead to an overestimation of the seasonal snow-covered area and an underestimation of the ELA/SLA. In such cases, the inferred boundary will correspond to the firn-ice boundary rather than the true snow-firn boundary (e.g., Fig. 10 in Aberle and others, 2025). Although snow and firn can also be visually difficult to distinguish in moderate-resolution (30 m) imagery (e.g., Rabatel and others, 2013; Larocca and others, 2024), we suggest that the larger bias between satellite-derived SLAs and field-measured ELAs (−146 m and −142 m), together with the very low bias between satellite- and manually derived SLAs (−0.8 m), indicates that in some cases the tool did not capture true end-of-ablation-season conditions rather than reflecting a systematic classification error of firn as snow.

In addition, our algorithm does not employ a time-varying DEM (as, to date, these data are not readily available) and instead uses either the ArcticDEM or COPDEM depending on the glacier location. Consequently, our approach cannot account for glacier surface lowering over time. This limitation is particularly relevant for the GEE tool-derived SLA observations, and the total and snow-covered area-elevation distributions. We therefore suggest that elevations derived from observations early in the record likely represent minimum estimates, whereas those derived toward the end of the record likely represent maximum estimates.

Glacier surfaces are most easily classified from satellite imagery when glacier geometry is simple and when shadowing from surrounding topography, cloud cover, and debris cover are limited (e.g., Aberle and others, 2025). Challenges arise for glaciers with complex geometries (e.g., multiple tributaries, icefall(s), or steep ridgelines along the glacier margin), frequent cloudiness, extensive debris cover and topographic shadowing (e.g., Loibl and others, 2025). Because our GEE tool is designed for global application, the workflow includes several features intended to manage these limitations as best as possible across a wide range of glacierized settings. Annual images are first filtered using user-defined thresholds for maximum cloud cover and minimum sun elevation, and scenes that do not meet these criteria are excluded. Further, the algorithm reduces topographic effects on reflectance using an Ekstrand correction based on terrain slope, aspect, and solar geometry. In addition, optional rock/water masking with user-selectable masking strength is provided to reduce misclassification of surrounding rock and water surfaces (including glacial lakes).

### *4.3. Use and value of the tool for glacier monitoring*

#### *4.3.1. Expansion of the observational record*

Field-based glacier observations are often not continuous, even for well-monitored glaciers (e.g., Zemp and others, 2009). Our space-based approach substantially increases the temporal completeness of glacier health observations for field-monitored glaciers, filling year-to-year temporal gaps in WGMS records ~63% of the time. WGMS observations of TA and SCA are particularly sparse relative to ELA. Across the 40 years and 60 glaciers in our study, the GEE tool provides 916 additional observations of

SCA and TA (equivalent to ~15 additional observations per glacier). This highlights the potential for space-based methods to complement in situ observations by improving the temporal completeness, and thus the overall quality, of glacier health records across multiple decades. However, we emphasize that tool-derived observations are not equivalent to field-based WGMS measurements and are best interpreted as a complementary record rather than a direct replacement for missing in situ observations.

The tool is designed and intended for application beyond the relatively small number of well-monitored glaciers studied here and has the potential to generate accessible, multi-decadal observations for individual glaciers of interest that are currently unmonitored. Thus, in the following sections we discuss the potential value and application of the tool and workflow for academic and non-academic users while acknowledging known limitations and challenges.

#### *4.3.2. Educational and non-academic use*

Our GEE tool is designed to support a wide range of users in gathering glacier health data for diverse applications, without the requirement of extensive coding knowledge or the internal structure of GEE. By removing these technical barriers to entry, the tool will make glaciological data more accessible across a range of educational and professional backgrounds. For example, we anticipate that this tool will be relevant in K-12 and higher education settings where it may be used to introduce students to concepts such as glacier and climate change, as well as Earth observation through hands-on exploration of remote sensing techniques.

We anticipate that our tool will also be particularly relevant within communities that are highly dependent on glacial meltwater (e.g. the Andes) and where accessible glacier monitoring data remains limited, creating difficulties for local populations and policymakers attempting to adapt and mitigate the impacts of glacier loss (Vuille and others, 2018). However, we acknowledge that the tool may not perform equally well in all glacierized settings (e.g., when shadowing from surrounding topography, cloud cover, and debris cover are extensive) and that classification errors may occur. We therefore recommend that users visually inspect annual image and classification quality, assess the timing of observations relative to the end of the mass-balance year, and review outlying results before interpretation when applying the tool to individual glaciers of interest.

#### *4.3.3. Academic use and potential for larger scale application*

We expect that the tool will be valuable to a wide range of users across academic subfields (e.g. environmental assessment, water resource management, and hazard assessment), supporting site-specific data analyses where field observations are unavailable. For example, time series may be used to evaluate local glacier change and its implications for downstream ecosystems; trends in local glacier SCA and SLA may inform assessments of seasonal meltwater availability and variability; and changes in local glacier extent may provide context for identifying evolving conditions associated with glacier-related hazards.

The workflow presented here also holds potential for upscaling (i.e., regional and global glacier assessment). Observational data are critically needed for the calibration and validation of glacier evolution models, and ultimately to improve projections of glacier change and its impacts. As noted by Wells and others (2025), observations of glacier change remain limited in both number and duration. Available records are sparse and relatively short compared to glacier response times and are therefore insufficient to robustly constrain model parameters. Regional and global application of the algorithm could substantially increase both the number and temporal range of glacier observations. However, we acknowledge and anticipate a number of challenges associated with large-scale application of the workflow. For example, selecting an appropriate month representative of the end of the mass balance year may be difficult for unmonitored glaciers (e.g., in tropical regions and for glaciers with summer accumulation). Further, difficulties may arise in regions with frequent or persistent cloud cover limiting the availability of suitable imagery. In addition, the tool has not been evaluated for heavily debris-covered

or marine-terminating glaciers. Finally, automated larger-scale (i.e., regional- and global-scaling) applications may not be possible within the GEE platform and would likely require additional computing resources (e.g., high-performance computing).

In addition to integration and comparison with glacier evolution models, larger-scale application of this workflow would also enable assessment of the degree of glacier disequilibrium with the current climate state (via the AAR metric). This disequilibrium and the associated committed glacier mass loss during the twenty-first century remains poorly constrained (e.g., Marzeion and others, 2020). Expanded observational records could also help assess the representativeness of field-based time series used to extrapolate glacier change to mountain ranges lacking in situ observations (e.g., Zemp and others, 2009).

## 5. Conclusions

Here we present a novel cloud-based algorithm for the automatic classification of glacier surfaces and derivation of four glacier health metrics—SCA, SLA, AAR, and TA—closely related to climate and glacier mass balance, designed to be applied to unmonitored glaciers of interest. We assess the performance of the tool using 60 glaciers worldwide with long-term field-based observational records from the WGMS, as well as manually delineated observations for the same glaciers. Even when accounting for between-glacier differences in size and elevation, we find overall strong agreement between manual and GEE-tool observations (SLA: $r = 0.77$, SCA: $r = 0.85$, TA $r = 0.64$, and AAR: $r = 0.82$), while a weaker agreement between WGMS and GEE-tool observations (SLA: $r = 0.18$, SCA: $r = 0.07$, TA $r = 0.05$, and AAR: $r = 0.11$) is likely reflective of differences in methodology and observation date. The tool also substantially improves the temporal completeness of the WGMS records, providing space-based observations ~63% of the time when WGMS records are missing. We anticipate that this tool will be relevant to a broad range of users and will allow academic and non-academic practitioners, including those with little to no coding or remote sensing experience, to easily obtain meaningful insights into glacier health for their areas of interest. Larger-scale application of the workflow could also provide critically needed multi-decadal observational records for calibration of glacier evolution models, while application to individual glaciers could supply communities with accessible datasets to monitor nearby glaciers and respond effectively to ongoing glacier change.

**Supplementary Material.** The supplementary material for this article can be found at *insert link here*.

**Data Availability Statement.** The GEE tool GUI and walkthrough instructions are available via GitHub at https://github.com/LamantiaKara/Glacier-Health-Tool. Supporting data are publicly available from the following sources: Glacier outlines (the glacier product and glacier complex product) are available from the Randolph Glacier Inventory version 7.0 (RGI7.0) at https://doi.org/10.5067/f6jmovy5navz (RGI Consortium, 2023); the ArcticDEM is available at https://doi.org/10.7910/DVN/3VDC4W (Porter and others, 2023); the Copernicus GLO-30 DEM is available at https://doi.org/10.5069/G9028PQB (European Space Agency, 2024), and Landsat imagery is available from the U.S. Geological Survey via several data portals (e.g., USGS EarthExplorer: https://earthexplorer.usgs.gov/).

**Acknowledgements.** This work was supported by a Royal Society Newton International Fellowship (NIFR1251037) to KAL. JML acknowledges support from UKRI Future Leaders Fellowship (MR/X02346X/1).

**Author Contributions.** All authors contributed to the methodology, based on initial ideas by KAL and LJL. KAL and JML wrote the GEE tool code with input from LJL and RA. LJL and KAL wrote the first draft. All authors contributed to editing and revision.

**Funding Statement.** This research is funded by the Royal Society through the Newton International Fellowship (NIFR1251037).

**Competing Interests.** The authors declare that they have no competing interests.

## References

**Aberle R**, Enderlin E, O'Neel S, Florentine C, Sass L, Dickson A and 2 others (2025) Automated snow cover detection on mountain glaciers using spaceborne imagery and machine learning. *The Cryosphere* **19**(4), 1675–1693.
**Baruah B**, Rajak R, Gupta A, Sharma K, Roy A, Yadav S and 4 others (2026) Disappearing glaciers of Sikkim Himalaya: a multi-decadal remote sensing analysis. *Journal of Earth System Science* **135**(2), 80.
**Benn D and Evans DJA** (2010) *Glaciers and Glaciation*. Hodder Education, London.
**Braithwaite RJ** and Müller F (1980) On the parameterization of glacier equilibrium line altitude. *IAHS Publication* **126**, 263–271.
**Calvin K**, Dasgupta D, Krinner G, Mukherji A, Thorne PW, Trisos C and 16 others (2023) *IPCC, 2023: Climate Change 2023: Synthesis Report.* Contribution of Working Groups I, II and III to the Sixth Assessment Report of the Intergovernmental Panel on Climate Change, IPCC, Geneva, Switzerland.
**Cogley JG**, Hock R, Rasmussen LA, Arendt AA, Bauder A, Braithwaite RJ and 5 others (2011) *Glossary of Mass Balance and Related Terms*. IHP-VII Technical Documents in Hydrology No. 86, IACS Contribution No. 2.
**Dozier J** (1989) Spectral signature of alpine snow cover from the Landsat Thematic Mapper. *Remote Sensing of Environment* **28**, 9–22.
**Durán-Alarcón C**, Gevaert CM, Mattar C, Jiménez-Muñoz JC, Pasapera-Gonzales JJ, Sobrino JA and 4 others (2015) Recent trends on glacier area retreat over the group of Nevados Caullaraju-Pastoruri (Cordillera Blanca, Peru) using Landsat imagery. *Journal of South American Earth Sciences* **59**, 19–26.
**Ekstrand S** (1996) Landsat TM-based forest damage assessment: correction for topographic effects. *Photogrammetric Engineering and Remote Sensing* **62**(2), 151–161.
**European Space Agency** (2024) Copernicus Global Digital Elevation Model [dataset]. Distributed by OpenTopography. (doi:10.5069/G9028PQB). Accessed 28 January 2026.
**Ficetola GF**, Marta S, Guerrieri A, Cantera I, Bonin A, Cauvy-Fraunié S and 10 others (2024) The development of terrestrial ecosystems emerging after glacier retreat. *Nature* **632**(8024), 336–342.
**Haeberli W and Whiteman C (2015)** Snow and ice-related hazards, risks, and disasters: a general framework. In Haeberli W and Whiteman C (eds.), *Snow and Ice-Related Hazards, Risks, and Disasters*, Academic Press, 1–34.
**Hall DK and Riggs GA** (2010) Normalized-difference snow index (NDSI). In Singh VP, Singh P and Haritashya UK (eds.), *Encyclopedia of Snow, Ice and Glaciers*, Springer.
**Hock R**, Bliss A, Marzeion B, Giesen RH, Hirabayashi Y, Huss M and 2 others (2019) GlacierMIP – a model intercomparison of global-scale glacier mass-balance models and projections. *Journal of Glaciology* **65**(251), 453–467.
**Hugonnet R**, McNabb R, Berthier E, Menounos B, Nuth C, Girod L and 5 others (2021) Accelerated global glacier mass loss in the early twenty-first century. *Nature* **592**(7856), 726–731.
**Huss M** and Hock R (2018) Global-scale hydrological response to future glacier mass loss. *Nature Climate Change* **8**(2), 135–140.
**Huss M**, Fischer M, Linsbauer A and Bauder A (2025) Continuous monitoring of a glacier's extinction. *Annals of Glaciology* **66**, e27.
**Immerzeel WW**, Lutz AF, Andrade M, Bahl A, Biemans H, Bolch T and 14 others (2020) Importance and vulnerability of the world's water towers. *Nature* **577**(7790), 364–369.
**Larocca LJ**, Twining-Ward M, Axford Y, Schweinsberg AD, Larsen SH, Westergaard-Nielsen A and 4 others (2023) Greenland-wide accelerated retreat of peripheral glaciers in the twenty-first century. *Nature Climate Change* **13**(12), 1324–1328.
**Larocca LJ**, Lea JM, Erb MP, McKay NP, Phillips M, Lamantia KA and Kaufman DS (2024) Arctic glacier snowline altitudes rise 150 m over the last 4 decades. *The Cryosphere* **18**(8), 3591–3611.
**Loibl D**, Richter N and Grünberg I (2025) Remote sensing-derived time series of transient glacier snowline altitudes for High Mountain Asia, 1985–2021. *Scientific Data* **12**(1), 103.
**Malca UFG**, Solano LNY, Carranza SVC, Alvarez DGC, Quispe FCQ, García JAC and Mark BG (2025) The loss of glacier resilience due to climate change throughout the Cordillera Blanca, Peru between 1984 and 2023. *Quaternary Science Advances* **19**, 100286.
**Marzeion B**, Hock R, Anderson B, Bliss A, Champollion N, Fujita K and 9 others (2020) Partitioning the uncertainty of ensemble projections of global glacier mass change. *Earth's Future* **8**(7), e2019EF001470.

**Masson-Delmotte V**, Zhai P, Pirani A, Connors SL, Péan C, Berger S and 6 others (2021) *Climate Change 2021: The Physical Science Basis*. Contribution of Working Group I to the Sixth Assessment Report of the Intergovernmental Panel on Climate Change, Cambridge University Press.
**Meier MF** (1962) Proposed definitions for glacier mass budget terms. *Journal of Glaciology* **4**(33), 252–263.
**Mernild SH**, Pelto M, Malmros JK, Yde JC, Knudsen NT and Hanna E (2013) Identification of snow ablation rate, ELA, AAR and net mass balance using transient snowline variations on two Arctic glaciers. *Journal of Glaciology* **59**(216), 649–659.
**Moussavi M**, Pope A, Halberstadt ARW, Trusel LD, Cioffi L and Abdalati W (2020) Antarctic supraglacial lake detection using Landsat 8 and Sentinel-2 imagery: towards continental generation of lake volumes. *Remote Sensing* **12**(1), 134.
**Ohmura A and Boettcher M** (2022) On the shift of glacier equilibrium line altitude (ELA) under the changing climate. *Water* **14**(18), 2821.
**Otosaka IN**, Shepherd A, Ivins ER, Schlegel NJ, Amory C, van den Broeke M and 6 others (2022) Mass balance of the Greenland and Antarctic ice sheets from 1992 to 2020. *Earth System Science Data Discussions 2022*, 1–33.
**Otsu N** (1979) A threshold selection method from gray-level histograms. *IEEE Transactions on Systems, Man, and Cybernetics* **9**(1), 62–66.
**Pfeffer WT**, Arendt AA, Bliss A, Bolch T, Cogley JG, Gardner AS and 11 others (2014) The Randolph Glacier Inventory: a globally complete inventory of glaciers. *Journal of Glaciology* **60** (221), 537–552.
**Porter C**, Howat I, Noh MJ, Husby E, Khuvis S, Danish E and others (2023) ArcticDEM – Mosaics, Version 4.1 [dataset]. Harvard Dataverse. (doi:10.7910/DVN/3VDC4W).
**Rabatel A**, Bermejo A, Loarte E, Soruco A, Gomez J, Leonardini G and 2 others (2012) Can the snowline be used as an indicator of the equilibrium line and mass balance for glaciers in the outer tropics? *Journal of Glaciology* **58**(212), 1027–1036.
**Rabatel A**, Letréguilly A, Dedieu JP and Eckert N (2013) Changes in glacier equilibrium-line altitude in the western Alps from 1984 to 2010: evaluation by remote sensing and modeling of the morpho-topographic and climate controls. *The Cryosphere* **7**(5), 1455–1471.
**Racoviteanu AE**, Rittger K and Armstrong R (2019) An automated approach for estimating snowline altitudes in the Karakoram and Eastern Himalaya from remote sensing. *Frontiers in Earth Science* **7**, 220.
**Ramírez E**, Francou B, Ribstein P, Descloitres M, Guérin R, Mendoza J and 4 others (2001) Small glaciers disappearing in the tropical Andes: a case-study in Bolivia: Glaciar Chacaltaya (16°S). *Journal of Glaciology* **47**(157), 187–194.
**Rastner P**, Prinz R, Notarnicola C, Nicholson L, Sailer R, Schwaizer G and Paul F (2019) On the automated mapping of snow cover on glaciers and calculation of snow line altitudes from multi-temporal Landsat data. *Remote Sensing* **11**(12), 1410.
**RGI Consortium** (2023) Randolph Glacier Inventory – A Dataset of Global Glacier Outlines (NSIDC-0770, Version 7) [dataset]. National Snow and Ice Data Center, Boulder, Colorado, USA. (doi:10.5067/F6JMOVY5NAVZ). Accessed 27 January 2026.
**Riggs GA**, Hall DK and Salomonson VV (1994) A snow index for the Landsat Thematic Mapper and Moderate Resolution Imaging Spectroradiometer. *Proceedings of IGARSS'94 – 1994 IEEE International Geoscience and Remote Sensing Symposium* **4**, 1942–1944.
**Rounce DR**, Hock R, Maussion F, Hugonnet R, Kochtitzky W, Huss M and 6 others (2023) Global glacier change in the 21st century: every increase in temperature matters. *Science* **379**(6627), 78–83.
**Santofimia E**, López-Pamo E, Palomino EJ, González-Toril E and Aguilera Á (2017) Acid rock drainage in Nevado Pastoruri glacier area (Huascarán National Park, Perú): hydrochemical and mineralogical characterization and associated environmental implications. *Environmental Science and Pollution Research* **24**(32), 25243–25259.
**Schuster L**, Rounce DR and Maussion F (2023) Glacier projections sensitivity to temperature-index model choices and calibration strategies. *Annals of Glaciology* **64**(92), 293–308.
**Serrano RB**, Soria A, Cusicanqui D, Rojas S, Torres G, Rivadeneira A and 3 others (2026) In memory of Carihuairazo, a recently disappeared ice cap in the inner tropics. *Annals of Glaciology* **67**, e14.
**The GlaMBIE Team** (2025) Community estimate of global glacier mass changes from 2000 to 2023. *Nature* **639**, 382–388. (doi:10.1038/s41586-024-08545-z).
**Van Tricht L**, Zekollari H, Huss M, Rounce DR, Schuster L, Aguayo R and 4 others (2025) Peak glacier extinction in the mid-twenty-first century. *Nature Climate Change*, 1–5. (doi: 10.1038/s41558-025-02513-9)
**Vuille M**, Carey M, Huggel C, Buytaert W, Rabatel A, Jacobsen D and 6 others (2018) Rapid decline of snow and ice in the tropical Andes – impacts, uncertainties and challenges ahead. *Earth-Science Reviews* **176**, 195–213.

**Warren SG** (2019) Optical properties of ice and snow. *Philosophical Transactions of the Royal Society A: Mathematical, Physical and Engineering Sciences* **377**(2146).
**Wells A**, Tober BS, Child SF, Rounce DR, Loso MG, Hults CP and 4 others (2025) An 85-year record of glacier change and refined projections for Kennicott and Root Glaciers, Alaska. *Nature Communications* **16**(1), 7835.
**WGMS** (2023) *Global Glacier Change Bulletin No. 5 (2020–2021)*. Zemp M, Gärtner-Roer I, Nussbaumer SU, Welty EZ, Dussaillant I and Bannwart J (eds.). World Glacier Monitoring Service, Zurich, Switzerland. (doi:10.5904/wgms-fog-2023-09).
**WGMS** (2024) Fluctuations of Glaciers Database [dataset]. World Glacier Monitoring Service, Zurich, Switzerland. (doi:10.5904/wgms-fog-2024-01).
**Zemp M**, Hoelzle M and Haeberli W (2009) Six decades of glacier mass-balance observations: a review of the worldwide monitoring network. *Annals of Glaciology* **50**(50), 101–111.

## Figure Captions

**Figure 1.** Global glacier locations (pink polygons) and locations of the 60 field-monitored glaciers from the World Glacier Monitoring Service (WGMS) used for tool validation and error estimation (black dots). Shaded polygons with thin gray edges represent the 19 first-order regions of the Randolph Glacier Inventory (RGI version 7.0; RGI Consortium, 2023).

**Figure 2.** Indicators of glacier health included in the Google Earth Engine (GEE) tool. The snow-covered area (SCA; 1); the snowline altitude (SLA; 2); the ablation area (3), the total visible ice area (TA; 1+3); and the accumulation-area ratio (AAR; 1/(1+3)).

**Figure 3.** Imagery acquisition month relative to the target month for each of the 60 study glaciers over the 1985–2024 observation period. White squares denote the target month, with a color gradient indicating the number of images acquired per month (left), and a bar chart showing the percentage of images acquired within the target month (right).

**Figure 4.** Example outputs for the Gulkana Glacier, Alaska. (a) Histogram of Ekstrand-corrected NIR surface reflectance (unitless) for a single end-of-summer Landsat scene, with the Otsu-derived threshold (yellow line) separating the bimodal distribution of snow (red) and ice (blue). (b) Resulting delineations of total glacier area (TA; blue) and snow-covered area (SCA; red) used in subsequent calculations of AAR and SLA.

**Figure 5.** Comparison of the GEE tool–derived glacier health metrics with manually digitized values (top row; panels a–d) and WGMS observations (bottom row; panels e–h). Metrics shown include snowline altitude/equilibrium-line altitude (SLA/ELA), snow-covered area (SCA), total glacier area (TA), and accumulation-area ratio (AAR). SLA/ELA is expressed as an anomaly (m) relative to each glacier's median tool-derived SLA. SCA and TA are expressed as ratios relative to each glacier's median tool-derived values to reduce the influence of between-glacier differences in size. AAR is shown in raw unitless form. Solid gray lines show the 1:1 relationship, dashed orange lines show linear regression fits.

**Figure 6.** Comparison of GEE tool-derived (pink) and WGMS-derived (blue) glacier health metrics and their relationships with annual mass balance. (a) Median percent change in TA relative to the 1985–2024 baseline summarized across the 60 study glaciers, with shaded bands indicating the interquartile range (IQR). (b and c) Distribution of glacier-level Pearson correlation coefficients ($r$) between b) SCA (% change) and annual mass balance, and c) SLA/ELA (anomaly) and annual mass balance. Colored dotted lines denote the median value. (d–f) Scatter plots of annual mass balance (m w.e.) versus (d) TA (% change), (e) SCA (% change), and (f) SLA/ELA (anomalies), with linear fits shown for GEE and WGMS.

**Figure 7.** Number of years within the 40-year period (1985-2024) with field-based only (WGMS; blue), space-based only (GEE tool; orange), and overlapping (GEE tool and WGMS; purple) observations of snow-covered area (SCA) for each assessed glacier.

## Formatted Tables

**Table 1.** Imagery acquisition parameters and processing options

| Panel Heading | Input Variable | Options |
|---|---|---|
| *Collect Imagery* | Glacier Name | Any (e.g. Gulkana) |
| | Start Year | 1985 to Present Year |
| | End Year | 1985 to Present Year |
| | Target Month | January through December (1-12) |
| | Max Cloud Cover | 0 to 100% (increments of 5) |
| | Min Sun Angle | 0 to 90 degrees (increments of 5) |
| *Processing Options* | DEM Source | COPDEM or Arctic DEM |
| | Rock/Water Masking Strength | 'Off', 'Light', 'Moderate', or 'High' |

**Table 2.** Validation and uncertainty of GEE tool-derived glacier health metrics

| | GEE tool versus Field Obs. (WGMS) | | | | | | GEE tool versus Manual Satellite Obs. | | | | | |
|---|---|---|---|---|---|---|---|---|---|---|---|---|
| *Metric* | *n* | Bias | RMSE | MAE | *r* | Median abs % diff | *n* | Bias | RMSE | MAE | *r* | Median abs % diff |
| *SLA/ELA (m)* | 1323; 1212 | -146.0; -142.0 | 238.0; 235.0 | 181.0; 179.0 | 0.99; 0.99 | 6; 6 | 240 | -0.8 | 88.2 | 42.0 | 0.99 | 1 |
| *SCA ($km^2$)* | 645 | 2.3 | 11.3 | 2.9 | 0.89 | 53 | 240 | 0.2 | 1.8 | 0.7 | 0.99 | 7 |
| *TA ($km^2$)* | 645 | 0.1 | 6.2 | 1.6 | 0.97 | 13 | 240 | -0.3 | 1.4 | 0.6 | 0.99 | 3 |

Validation statistics for the GEE tool-derived glacier health metrics compared with field-based observations (left) and with manual digitizations (right). *n* denotes the number of paired observations; RMSE is the root-mean-square error; MAE is the mean absolute error; *r* is the Pearson correlation coefficient, and Median abs % diff is the median absolute percent difference (%). We note that: AAR is not included as it is derived from the SCA and TA; the SLA/ELA row has two values representing the tool-derived SLA values compared with (1) ELA values from the WGMS (WGMS, 2024) and (2) ELA values reported in Ohmura and Boettcher (2022); and all statistics were computed from absolute values.

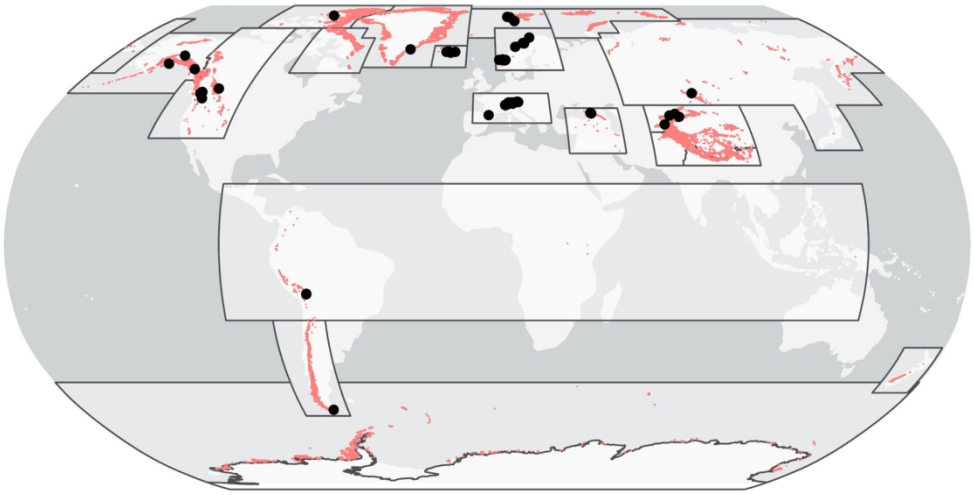

Figure 1. Global glacier locations (pink polygons) and locations of the 60 field-monitored glaciers from the World Glacier Monitoring Service (WGMS) used for tool validation and error estimation (black dots). Shaded polygons with thin gray edges represent the 19 first-order regions of the Randolph Glacier Inventory (RGI version 7.0; RGI Consortium, 2023).

240x127mm (300 x 300 DPI)

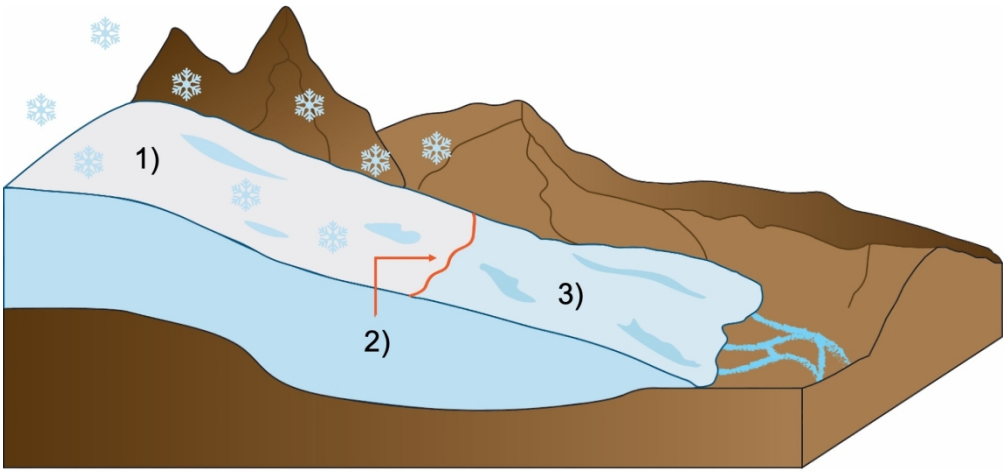


Figure 2. Indicators of glacier health included in the Google Earth Engine (GEE) tool. The snow-covered area (SCA; 1); the snowline altitude (SLA; 2); the ablation area (3), the total visible ice area (TA; 1+3); and the accumulation-area ratio (AAR; 1/(1+3)).

338x190mm (144 x 144 DPI)

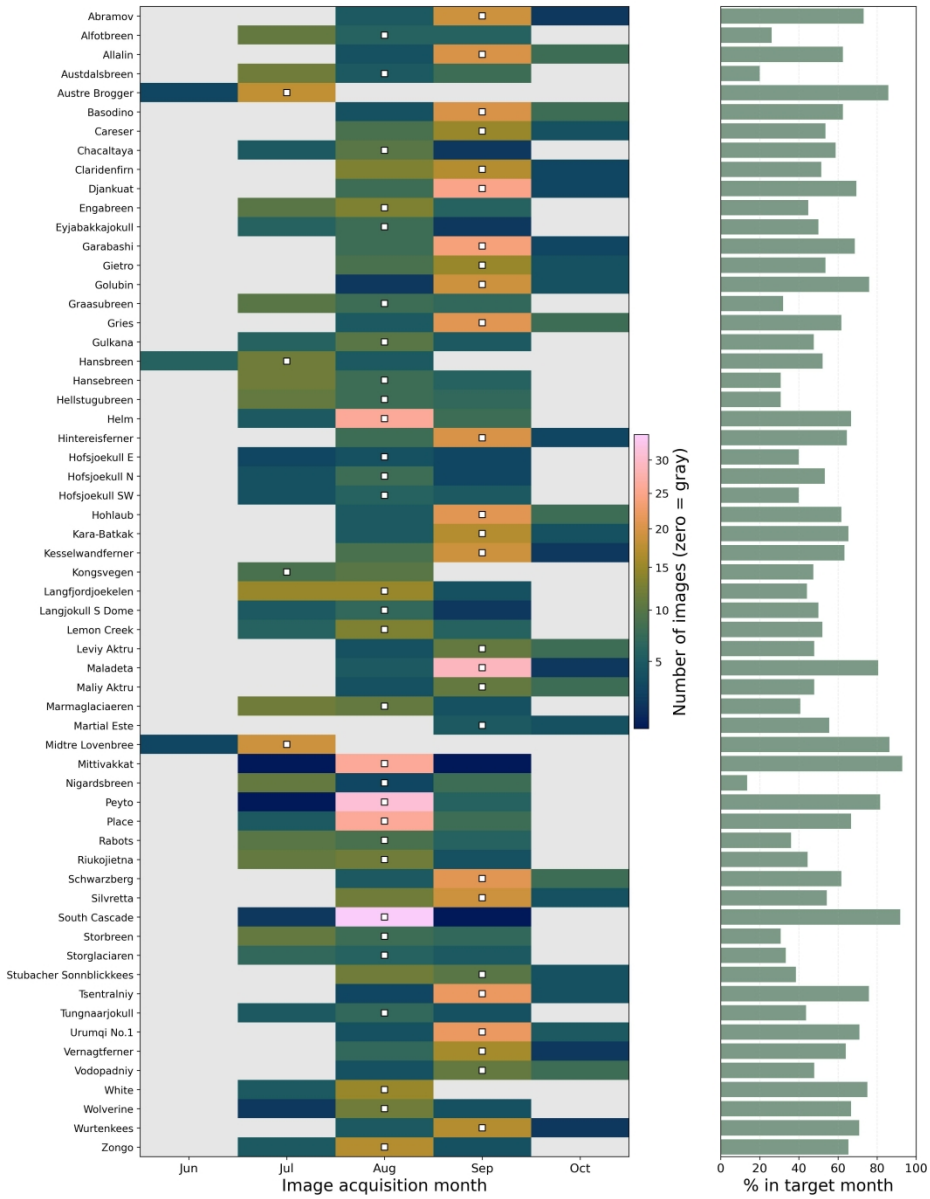


Figure 3. Imagery acquisition month relative to the target month for each of the 60 study glaciers over the 1985–2024 observation period. White squares denote the target month, with a color gradient indicating the number of images acquired per month (left), and a bar chart showing the percentage of images acquired within the target month (right).

358x460mm (300 x 300 DPI)

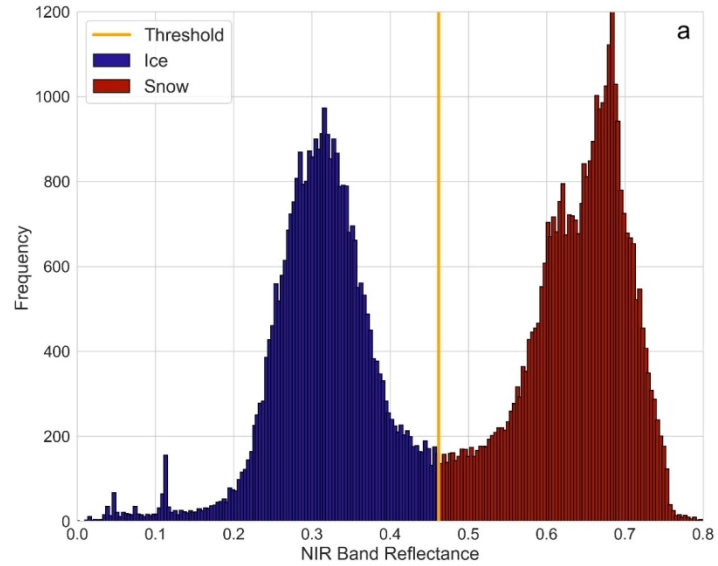


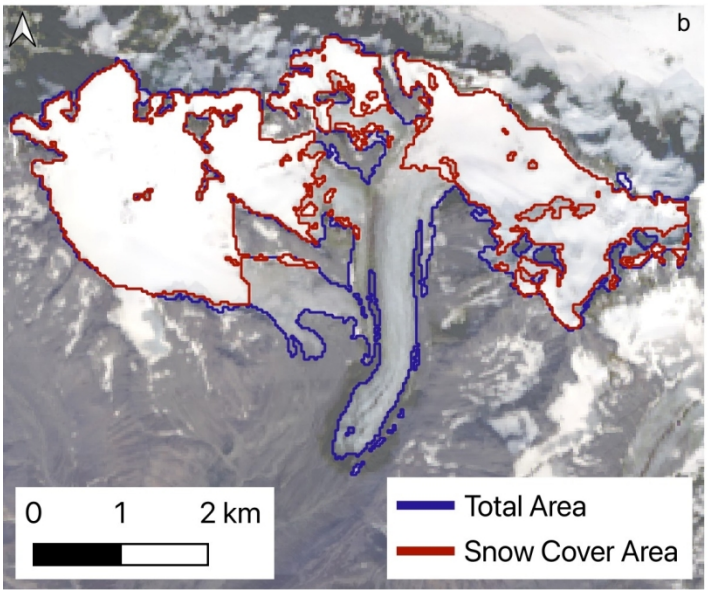


Figure 4. Example outputs for the Gulkana Glacier, Alaska. (a) Histogram of Ekstrand-corrected NIR surface reflectance (unitless) for a single end-of-summer Landsat scene, with the Otsu-derived threshold (yellow line) separating the bimodal distribution of snow (red) and ice (blue). (b) Resulting delineations of total visible ice area (TA; blue) and snow-covered area (SCA; red) used in subsequent calculations of AAR and SLA

261x434mm (118 x 118 DPI)

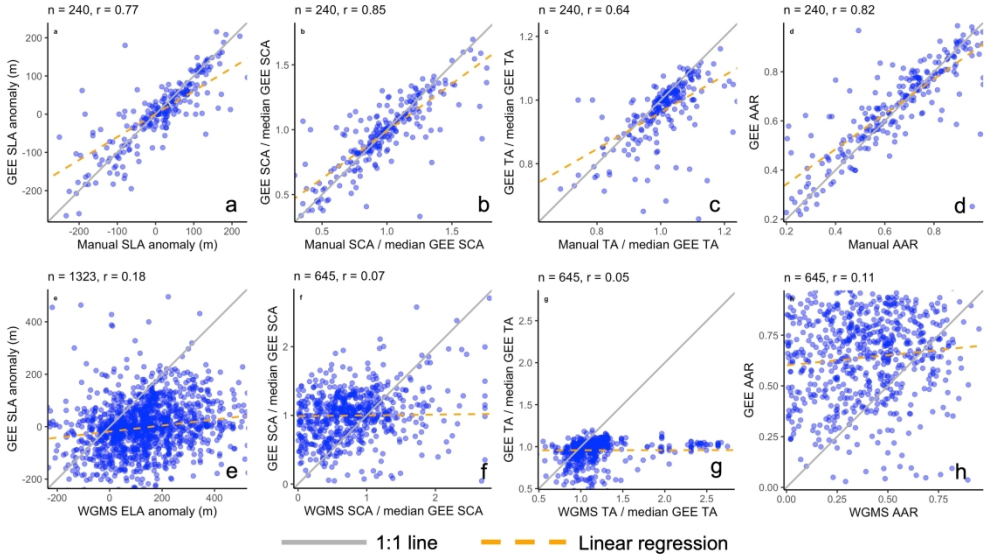


Figure 5. Comparison of the GEE tool–derived glacier health metrics with manually digitized values (top row; panels a–d) and WGMS observations (bottom row; panels e–h). Metrics shown include snowline altitude/equilibrium-line altitude (SLA/ELA), snow-covered area (SCA), total glacier area (TA), and accumulation-area ratio (AAR). SLA/ELA is expressed as an anomaly (m) relative to each glacier's median tool-derived SLA. SCA and TA are expressed as ratios relative to each glacier's median tool-derived values to reduce the influence of between-glacier differences in size. AAR is shown in raw unitless form. Solid gray lines show the 1:1 relationship, dashed orange lines show linear regression fits.

290x165mm (300 x 300 DPI)

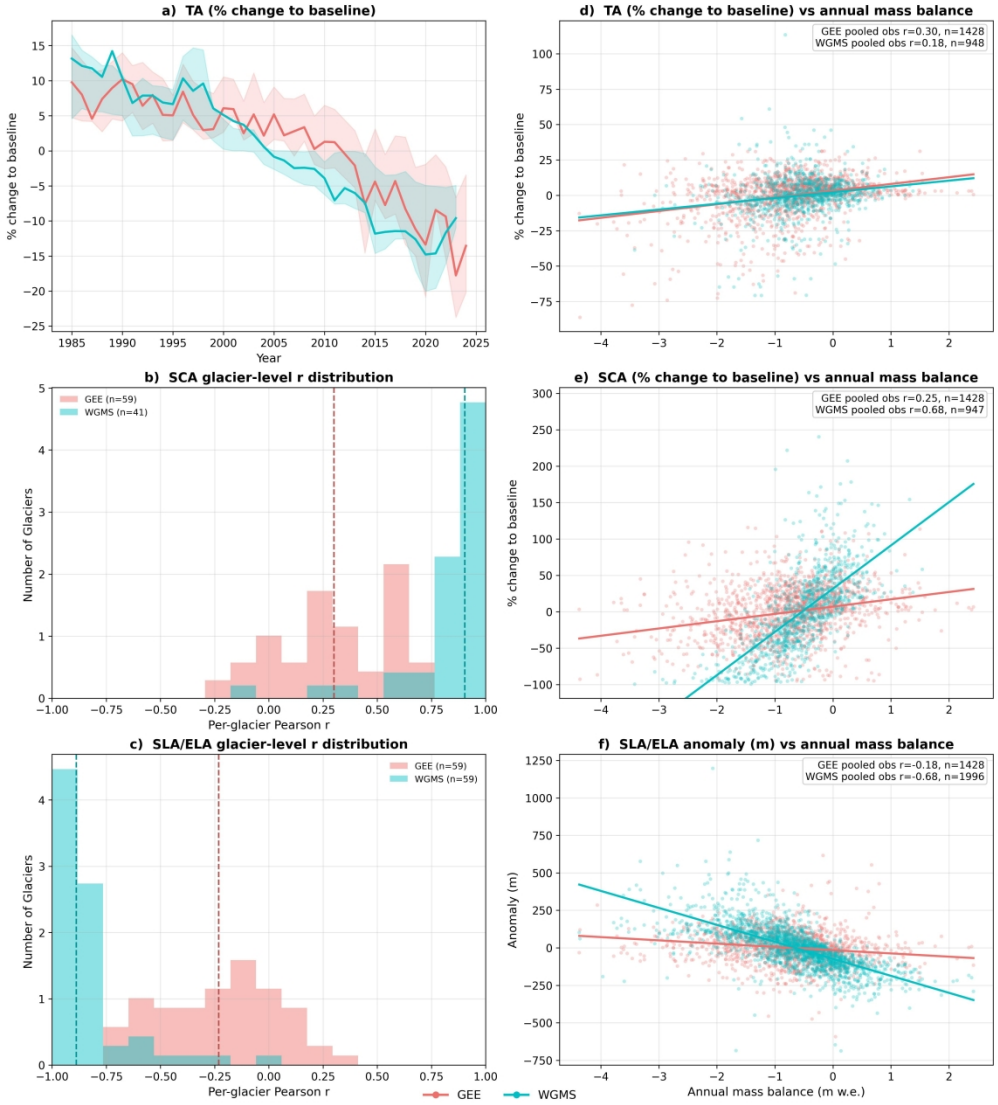


Figure 6. Comparison of GEE tool-derived (pink) and WGMS-derived (blue) glacier health metrics and their relationships with annual mass balance. (a) Median percent change in TA relative to the 1985–2024 baseline summarized across the 60 study glaciers, with shaded bands indicating the interquartile range (IQR). (b and c) Distribution of glacier-level Pearson correlation coefficients (r) between b) SCA (% change) and annual mass balance, and c) SLA/ELA (anomaly) and annual mass balance. Colored dotted lines denote the median value. (d–f) Scatter plots of annual mass balance (m w.e.) versus (d) TA (% change), (e) SCA (% change), and (f) SLA/ELA (anomalies), with linear fits shown for GEE and WGMS.

358x399mm (300 x 300 DPI)

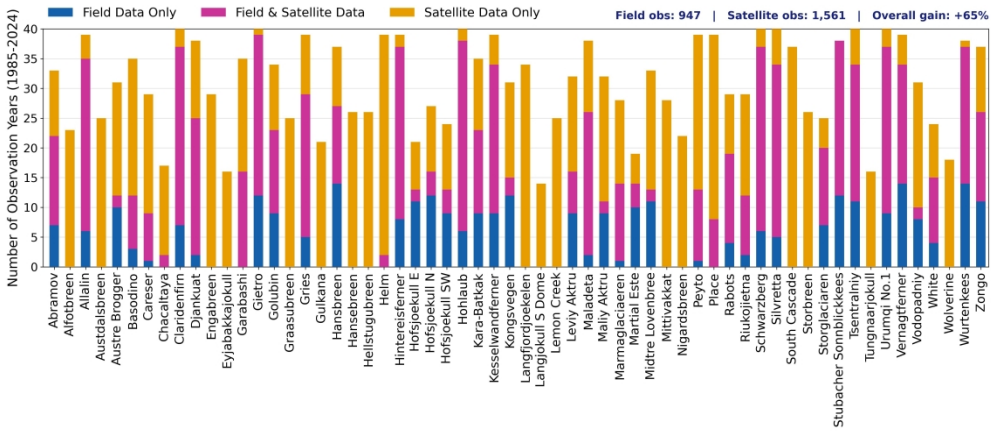


Figure 7. Number of years within the 40-year period (1985-2024) with field-based only (WGMS; blue), space-based only (GEE tool; orange), and overlapping (GEE tool and WGMS; purple) observations of snow-covered area (SCA) for each assessed glacier.

457x203mm (300 x 300 DPI)

*Supporting Information*

# A Google Earth Engine Tool for Mapping Key Metrics of Glacier Health from Space

Kara A. Lamantia[1*], Laura J. Larocca[2*], Rainey Aberle[3], Fabien Maussion[1], James M. Lea[4]

[1]*School of Geographical Sciences, University of Bristol, Bristol, UK*
[2]*School of Ocean Futures, Arizona State University, Tempe, AZ, USA*
[3]*Department of Geosciences, Boise State University, Boise, ID 83725, USA*
[4]*Department of Geography and Planning, University of Liverpool, Liverpool, UK*
*These authors contributed equally to this work

*Correspondence: Kara Lamantia <kara.lamantia@bristol.ac.uk>*

**Contents of this file**

- SI Table 1-2
- SI Figure 1-7

**SI Table 1.** The sixty glaciers analyzed with the Google Earth Engine tool and accompanying imagery acquisition parameters and processing options

| **Glacier Name** | **WGMS ID** | **Target Month** | **DEM Source** | **Rock/Water Masking Strength** | **# of years analyzed (1985–2024)** |
|---|---|---|---|---|---|
| Abramov | 732 | September | COPDEM | Off | 26 |
| Alfotbreen | 317 | August | COPDEM | Off | 23 |
| Allalin | 394 | September | COPDEM | Off | 34 |
| Austdalsbreen | 321 | August | COPDEM | Moderate | 25 |
| Austre Brogger | 292 | July | ArcticDEM | Off | 21 |
| Basodino | 463 | September | COPDEM | Off | 32 |
| Careser | 463 | September | COPDEM | Off | 29 |
| Chacaltaya | 1505 | August | COPDEM | Off | 17 |
| Claridenfirn | 2260 | September | COPDEM | Off | 33 |
| Djankuat | 726 | September | COPDEM | Off | 36 |
| Engabreen | 298 | August | ArcticDEM | Off | 29 |
| Eyjabakkajokull | 3069 | August | ArcticDEM | Off | 16 |

| | | | | | |
|---|---|---|---|---|---|
| Garabashi | 761 | September | COPDEM | Off | 35 |
| Gietro | 367 | September | COPDEM | Off | 28 |
| Golubin | 753 | September | COPDEM | Off | 25 |
| Graasubreen | 299 | August | COPDEM | Off | 25 |
| Griesgletscher | 359 | September | COPDEM | Off | 34 |
| Gulkana | 90 | August | ArcticDEM | Off | 21 |
| Hansbreen | 306 | July | ArcticDEM | Moderate | 23 |
| Hansebreen | 322 | August | ArcticDEM | Off | 26 |
| Hellstugubreen | 300 | August | COPDEM | Moderate | 26 |
| Helm | 45 | August | COPDEM | Moderate | 39 |
| Hintereisferner | 491 | Steptember | COPDEM | Off | 31 |
| Hofsjoekull E | 3088 | August | ArcticDEM | Off | 10 |
| Hofsjoekull N | 3089 | August | ArcticDEM | Off | 15 |
| Hofsjoekull SW | 3090 | August | ArcticDEM | Off | 15 |
| Hohlaub | 3332 | Steptember | COPDEM | Off | 34 |
| Kara-Batkak | 813 | Steptember | COPDEM | Off | 26 |
| Kesselwandferner | 507 | Steptember | COPDEM | Off | 30 |
| Kongsvegen | 1456 | July | ArcticDEM | Moderate | 19 |
| Langfjordjoekelen | 323 | August | ArcticDEM | Off | 34 |
| Langjokull S Dome (Hagafellsjoekull East) | 3101 | August | ArcticDEM | Off | 14 |
| Lemon Creek* | 3334 | August | ArcticDEM | Moderate | 26 |
| Leviy Aktru | 794 | September | COPDEM | Off | 23 |
| Maladeta | 942 | September | COPDEM | Off | 36 |
| Maliy Aktru | 795 | September | COPDEM | Off | 23 |
| Marmaglaciaeren | 1461 | August | COPDEM | Off | 27 |

| | | | | | |
|---|---|---|---|---|---|
| Martial Este | 2000 | September | COPDEM | Off | 9 |
| Midtre Lovenbree* | 291 | July | ArcticDEM | Off | 22 |
| Mittivakkat* | 1629 | August | ArcticDEM | Moderate | 28 |
| Nigardsbreen | 290 | August | COPDEM | Off | 22 |
| Peyto | 57 | August | COPDEM | Moderate | 38 |
| Place | 41 | August | COPDEM | Off | 39 |
| Rabots | 334 | August | COPDEM | Off | 25 |
| Riukojietna | 342 | August | ArcticDEM | Off | 27 |
| Schwarzberg | 395 | September | COPDEM | Low | 34 |
| Silvretta | 408 | September | COPDEM | Low | 35 |
| South Cascade | 205 | August | COPDEM | Low | 37 |
| Storbreen | 302 | August | COPDEM | Off | 26 |
| Storglaciaren | 332 | August | COPDEM | Off | 18 |
| Stubacher Sonnblickkees | 573 | September | COPDEM | Off | 26 |
| Tsentralniy (Tsentralniy Tuyuksuyskiy) | 817 | September | COPDEM | Off | 29 |
| Tungnaarjokull | 3126 | August | ArcticDEM | Off | 16 |
| Urumqi No.1 | 853 | September | COPDEM | Off | 31 |
| Vernagtferner | 489 | September | COPDEM | Off | 25 |
| Vodopadniy | 780 | September | COPDEM | Off | 23 |
| White | 0 | August | ArcticDEM | Off | 20 |
| Wolverine | 94 | August | ArcticDEM | Moderate | 18 |
| Wurtenkees | 545 | September | COPDEM | Off | 24 |
| Zongo | 26615 | August | COPDEM | Moderate | 26 |

*RGI glacier complex product was used (otherwise RGI glacier product was used).

**SI Table 2.** Landsat sensor information

| Sensor | Temporal Coverage | Utilized Bands | Spatial Resolution |
|---|---|---|---|
| Landsat 5 | 1985–2012 | B1 (Blue), B2 (Green), B3 (Red), B4 (NIR), B5 (SWIR1), B7 (SWIR2), B6 (Thermal) | 30 |
| Landsat 7 | 1999–2002* | B1 (Blue), B2 (Green), B3 (Red), B4 (NIR), B5 (SWIR1), B7 (SWIR2), B6 (Thermal) | 30 |
| Landsat 8 | 2013–present | B2 (Blue), B3 (Green), B4 (Red), B5 (NIR), B6 (SWIR1), B7 (SWIR2), B10 (Thermal) | 30 |
| Landsat 9 | 2021–present | B2 (Blue), B3 (Green), B4 (Red), B5 (NIR), B6 (SWIR1), B7 (SWIR2), B10 (Thermal) | 30 |

*Landsat 7 imagery acquired after 2002 was excluded in the tool due to the Scan Line Corrector (SLC) failure.

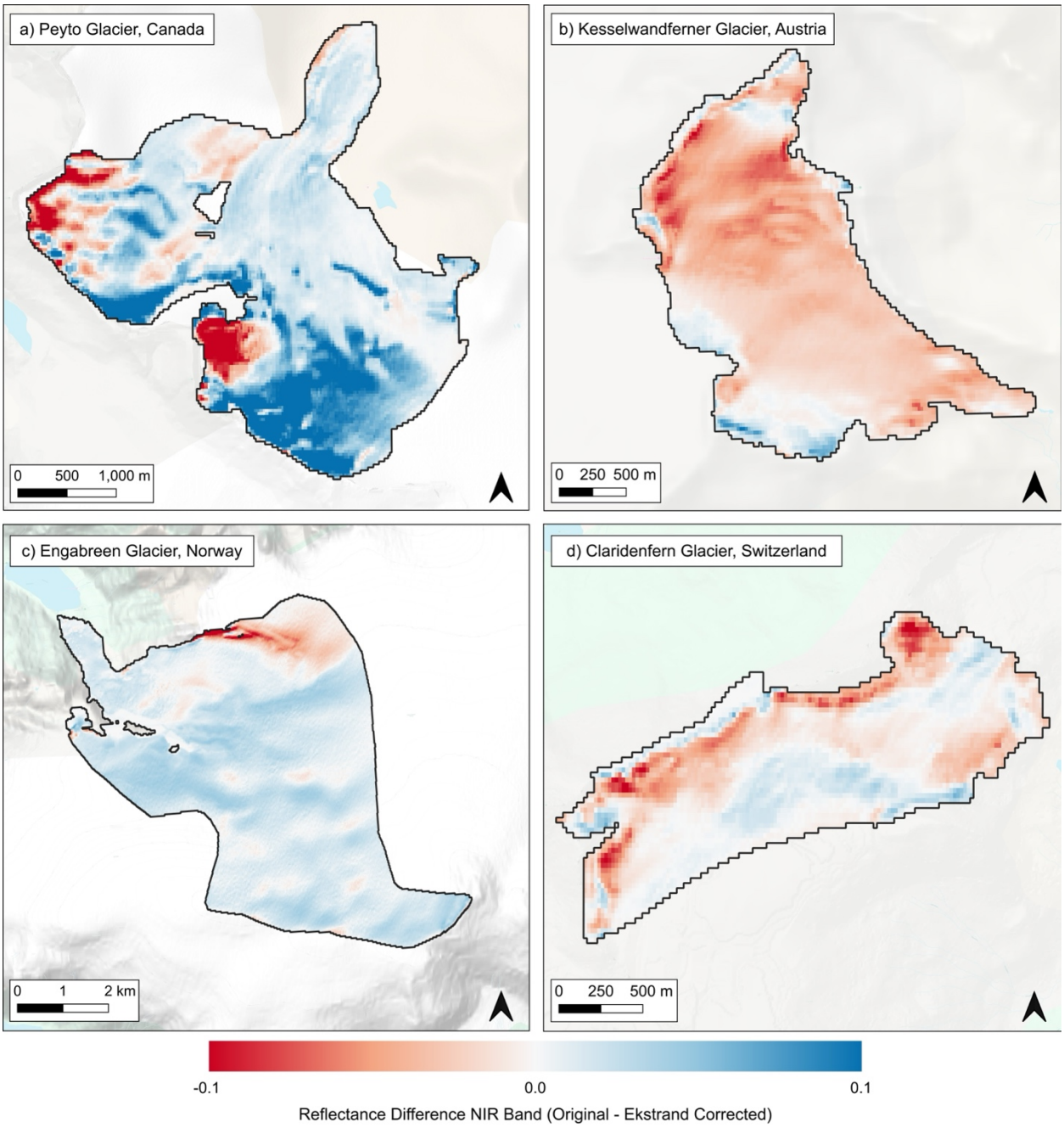


**SI Figure 1.** Pixel-wise difference between original Landsat surface reflectance (NIR Band) and reflectance after Ekstrand topographic correction. Positive values indicate reflectance reductions on sun-illuminated slopes, while negative values indicate increased reflectance in terrain shadow.

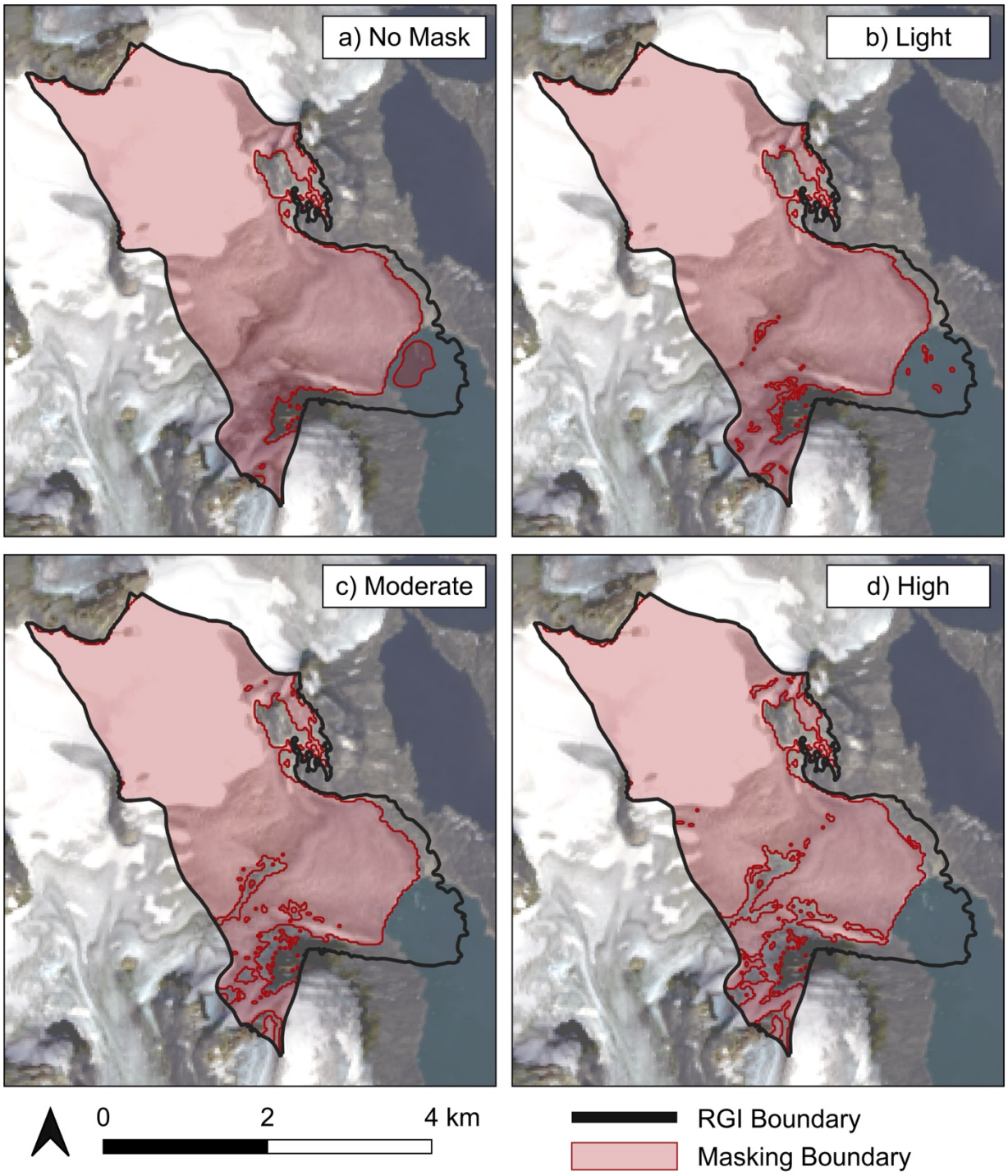


**SI Figure 2.** The four rock/water masking options available in the Google Earth Engine (GEE) tool (a) No Mask (Off), (b) Light, (c) Moderate, and (d) High shown on the Austdalsbreen glacier in Norway.

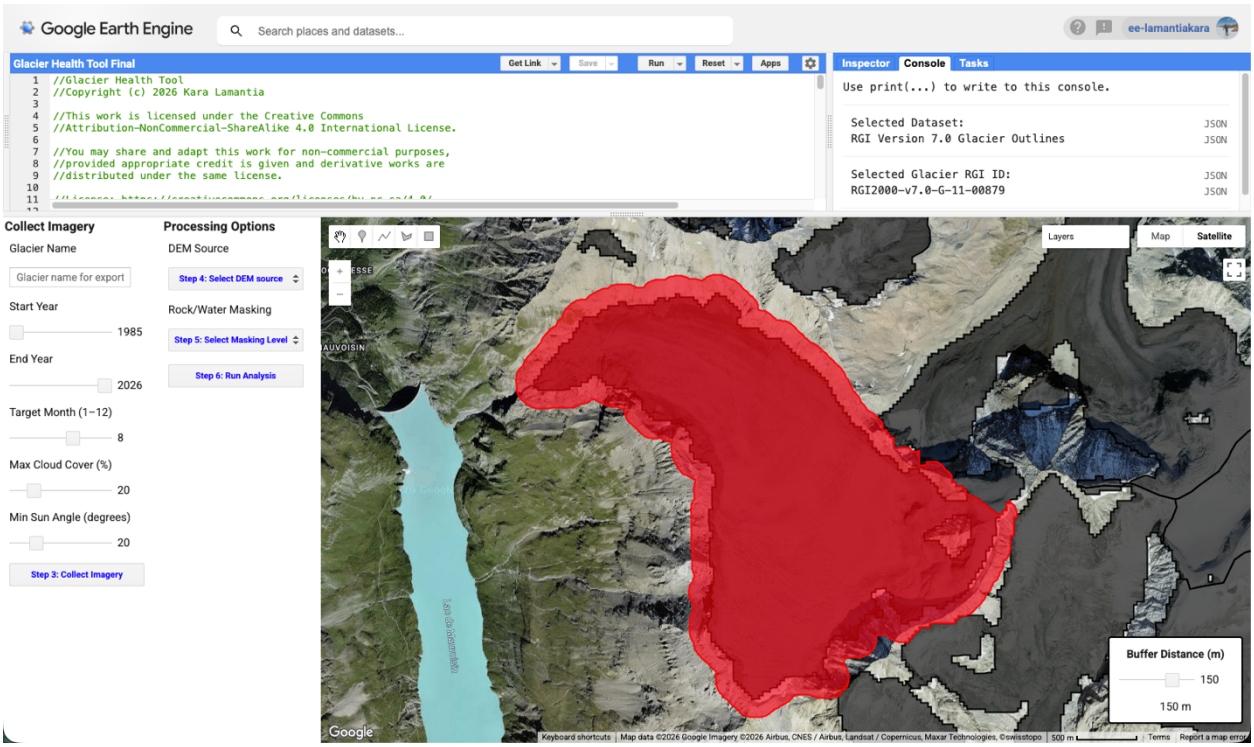


**SI Figure 3.** Snapshot of the GEE graphical user interface (GUI) after RGI selection is complete, with the buffer applied (here 150 m). Imagery acquisition parameters available for adjustment are shown in the left panel.

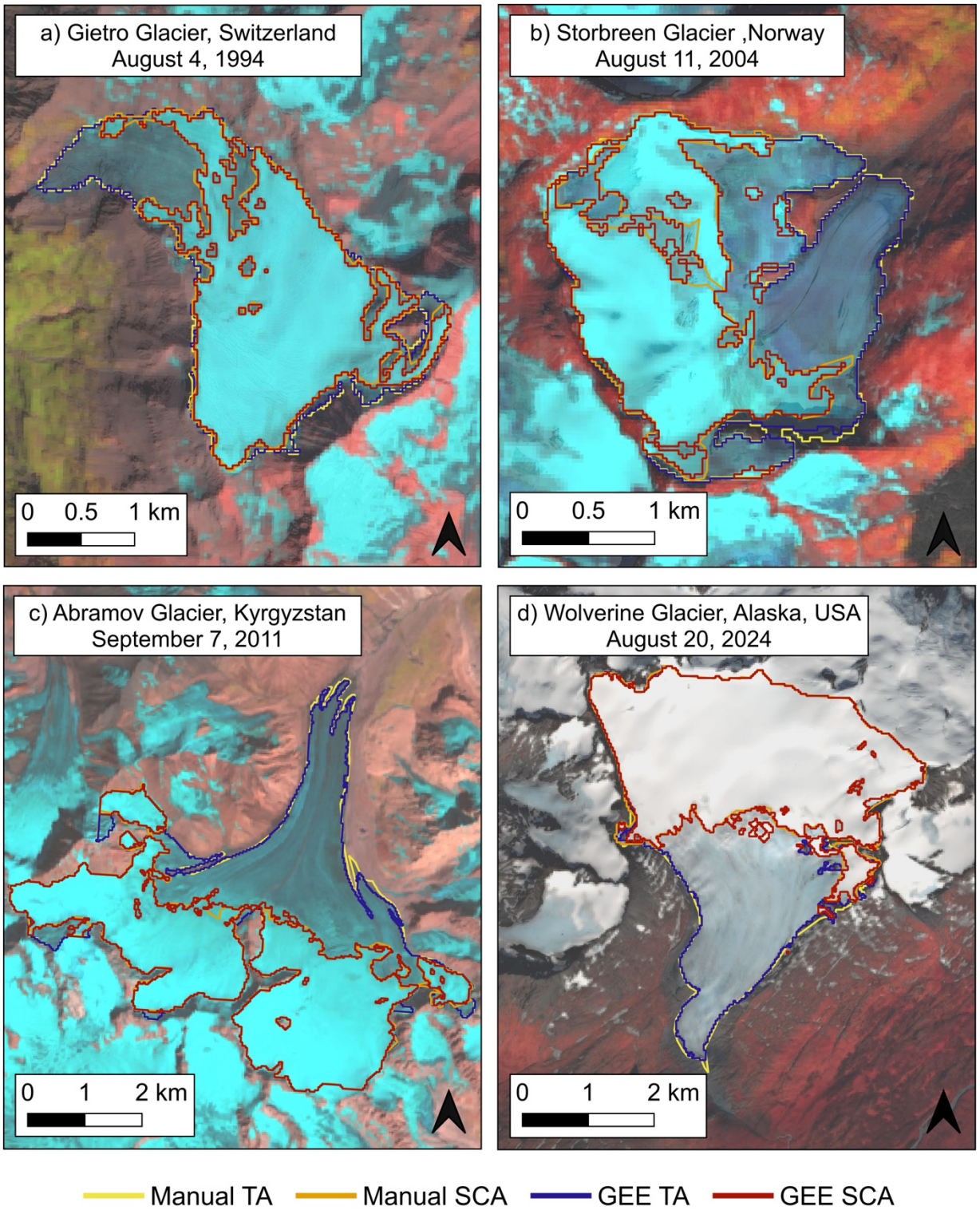


**SI Figure 4.** Google Earth Engine (GEE) tool-derived versus manually digitized snow-covered (red and orange, respectively) and total (blue and yellow, respectively) area for 4 example glaciers: (a) Gietro, (b) Storbreen, (c) Abramov, and (d) Wolverine. All glacier outlines are displayed with respective analyzed images in false color rendering.


**SI Figure 5.** Comparison of the ELA/SLA metric for eight individual glaciers: a) Engabreen, b) Garbashi, c) Hintereisferner, d) Kesselwandferner, e) Langfjordjoekelen, f) Peyto, g) Schwarzberg, and h) Vernagtferner. Shown are GEE-derived snowline altitudes, manual snowline altitudes, WGMS ELAs, and ELAs reported by Ohmura and Boettcher (2022) for all available observations between 1985 and 2024.

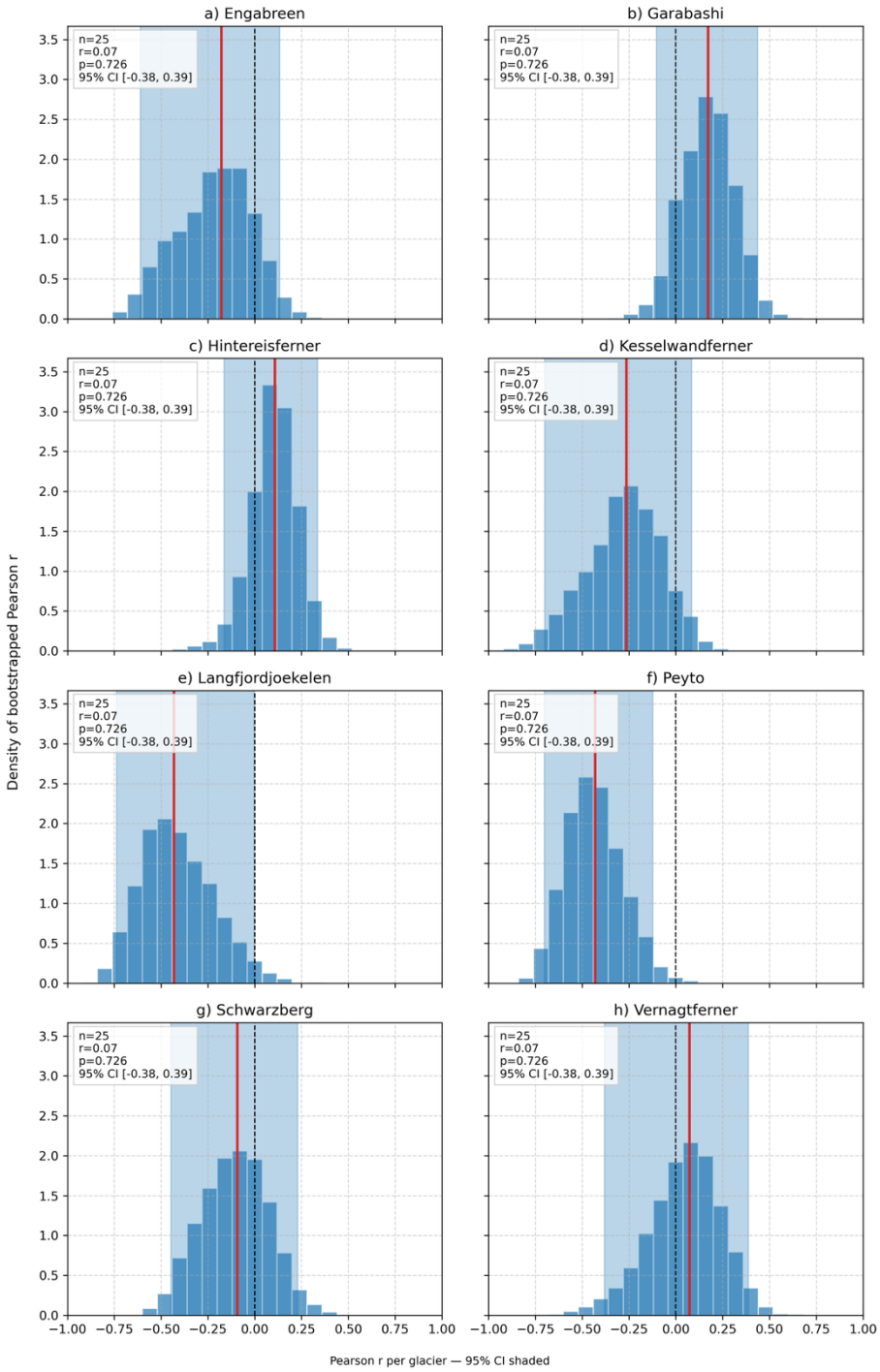


**SI Figure 6.** Distribution of glacier-level Pearson correlation coefficients (*r*) between SLA and annual mass balance for 8 example glaciers. The solid red line denotes the median value and the dotted black line denotes 0. Light blue shading shows the 95% confidence interval.

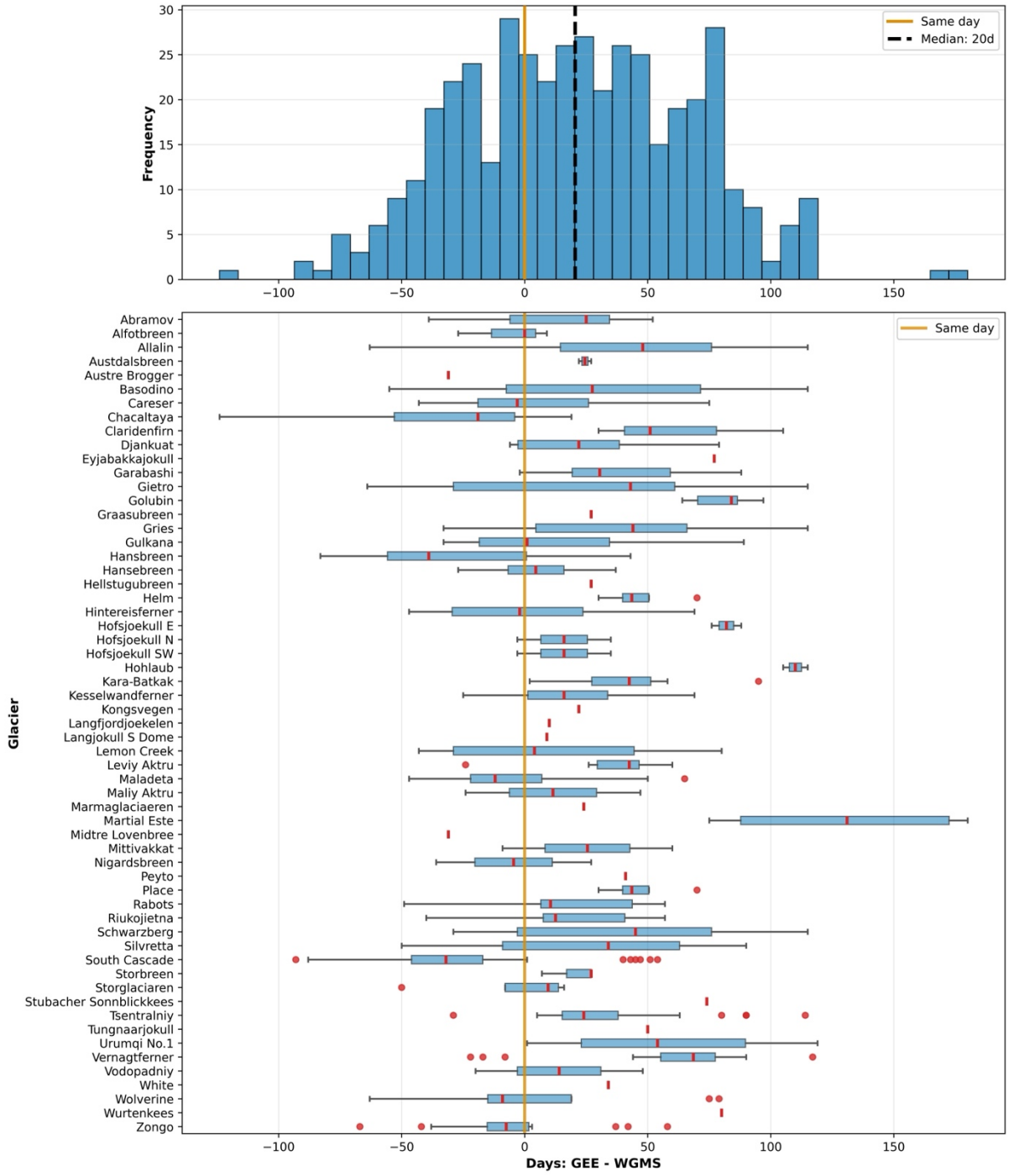


**SI Figure 7.** Comparison of the timing of WGMS field-based observations and GEE image acquisition date. Only a subset of WGMS records included full dates (day, month, and year; from the *SURVEY_DATE* column in *state.csv*), yielding 436 comparisons across 59 glaciers. The mean temporal offset (GEE − WGMS) is 20.8 days (median: 20.5 days; standard deviation: 46.2 days). We note that several glaciers (Austre Brogger, Eyjabakkajokullm Graasubreen, Kongsvegen, Langfjordjoekelen, Langjokull S Dome, Marmaglaciaeren, Midtre Lovenbree, Peyto, Stubacher Sonnblickkees, Tungnaarjokull, White, and Wurtenkees) had only a single comparison.